Review Article

Nano Research
2024, 17(5): 3516–3532

ISSN 1998-0124 CN 11-5974/O4
https://doi.org/10.1007/s12274-023-6310-x

Emerging strategies and developments in oxygen reduction reaction using high-performance platinum-based electrocatalysts

Asad Ali[1], Aatto Laaksonen[1,2,3,4], Guo Huang[1], Shahid Hussain[1], Shuiping Luo[5], Wen Chen[5], Pei Kang Shen[6] (✉), Jinliang Zhu[6] (✉), and Xiaoyan Ji[1] (✉)

[1] *Energy Engineering, Division of Energy Science, Luleå University of Technology, 97187 Luleå, Sweden*
[2] *Department of Materials and Environmental Chemistry, Arrhenius Laboratory, Stockholm University, SE-10691 Stockholm, Sweden*
[3] *Center of Advanced Research in Bionanoconjugates and Biopolymers, "Petru Poni" Institute of Macromolecular Chemistry, Iasi 700469, Romania*
[4] *State Key Laboratory of Materials-Oriented and Chemical Engineering, Nanjing Tech University, Nanjing 211816, China*
[5] *College of Materials Science and Engineering, Shenzhen University, Shenzhen 518060, China*
[6] *School of Resources, Environment and Materials, State Key Laboratory of Processing for Non-ferrous Metal and Featured Materials, Guangxi University, Nanning 530004, China*

Received: 20 September 2023 / **Revised:** 20 September 2023 / **Accepted:** 2 November 2023

ABSTRACT

The global practical implementation of proton exchange membrane fuel cells (PEMFCs) heavily relies on the advancement of highly effective platinum (Pt)-based electrocatalysts for the oxygen reduction reaction (ORR). To achieve high ORR performance, electrocatalysts with highly accessible reactive surfaces are needed to promote the uncovering of active positions for easy mass transportation. In this critical review, we introduce different approaches for the emerging development of effective ORR electrocatalysts, which offer high activity and durability. The strategies, including morphological engineering, geometric configuration modification via supporting materials, alloys regulation, core–shell, and confinement engineering of single atom electrocatalysts (SAEs), are discussed in line with the goals and requirements of ORR performance enhancement. We review the ongoing development of Pt electrocatalysts based on the syntheses, nanoarchitecture, electrochemical performances, and stability. We eventually explore the obstacles and research directions on further developing more effective electrocatalysts.

KEYWORDS

oxygen reduction reaction (ORR), Pt-based electrocatalysts, proton exchange membrane fuel cells (PEMFCs), morphology and alloys strategies, single atom electrocatalysts (SAEs)

1 Introduction

Global energy needs are estimated to grow up 36% by the year 2030 [1]. Despite the availability of modern technology, massive energy generation and consumption continue to rely mainly on fossil fuels [2, 3]. But the dependence on fossil fuels can have long-term climatic consequences, and with limited reserves, it is not a sustainable source [4, 5]. In this context, eco-friendly and renewable energy systems such as fuel cells technology offer a viable alternative. Fuel cells transform the chemical energy of oxidants and fuels into electric energy, producing only water and heat [6, 7]. They require a continuous fuel and oxidant supply but do not need recharging [8]. The benefits of fuel cells include their high efficiency and the availability of unlimited sources of reactants with no environmental pollution [9]. As such, fuel cells are ideal for powering portable electronics, electric vehicles, trains, and high-end energy storage systems and are expected to have extensive commercial applications [10]. Among fuel cell classification, the proton exchange membrane fuel cells (PEMFCs) have been effectively designed for vehicles and transportable electronics [11]. PEMFCs are particularly suitable for use in buses and automobiles, and they offer several features compared to electric vehicles driven by a battery, such as low operational temperatures, high power density, fast kick-off, and outstanding durability [12]. With these benefits, fuel cell technology has the potential to overcome energy supply issues, reduce environmental pollution, and create a clean environment [13].

The PEMFCs consist of three essential components: the cathode, anode, and membrane (Fig. 1). During the operation of PEMFCs, the hydrogen fuel is oxidized at the surface of the anode to generate proton ions (H^+) and electrons (e^-). These H^+ ions then move through the proton exchange membranes to the cathode direction, where they combine with oxygen to produce zero-carbon water molecules [14]. Although theoretical calculations offer tremendous potential for PEMFCs in addressing global warming and climate change issues, many challenges impede the profitable and economical launch of PEMFCs.[15] Especially, cathodic oxygen reduction reaction (ORR) requires more activation energy owing to the high stability of atmospheric oxygen molecules, which results in slow ORR kinetics that impedes the overall efficiency of PEMFCs [16]. Therefore, significant investment and exploration of cost-effective alternative strategies for ORR are demanded to reduce the overpotential and improve the energy conversion efficiency [17].

Address correspondence to Xiaoyan Ji, xiaoyan.ji@ltu.se; Pei Kang Shen, pkshen@gxu.edu.cn; Jinliang Zhu, jlzhu85@163.com

清華大學出版社 Tsinghua University Press Springer

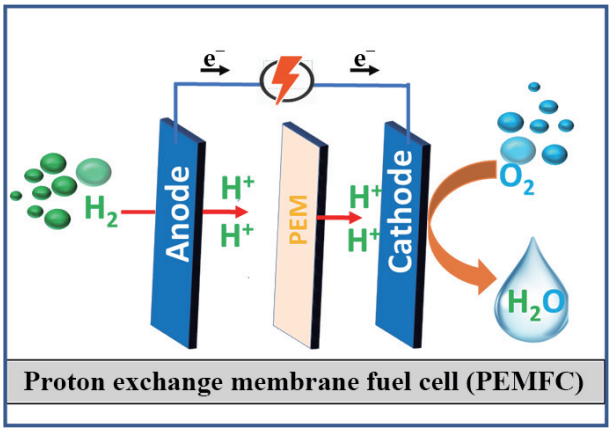

Figure 1 Schematic of the PEMFC.

Pt loaded on carbon is the current most used electrocatalyst for PEMFC cathodes [18]. However, its poor activity and limited durability impede its application at a global scale, as the small and active Pt nanoparticles (NPs) are exposed to electrolytic conditions that cause their dissolution and corrosion [19, 20]. Furthermore, carbon-support corrodes at high voltage, separating Pt NPs and reducing the integrity and durability of the whole approach [21]. The elevated price, scarcity, and predisposition to poisoning limit its widespread commercial application in PEMFCs [22]. Although the activity of non-precious-based electrocatalysts is steadily advancing, the potential of Pt-based electrocatalysts remains unparalleled [23], where how to decrease the Pt utilization in cathodic ORR is another challenge to commercialize the PEMFCs technology [24]. Various strategies, including controlling the surface and morphology, alloying, supporting, and single-atom strategies [25], have been suggested to optimize the morphology, composition, and electron structure of Pt-made composites and tune their adsorption properties to achieve higher levels of activity and durability.

Several review articles [25–27] have been published on Pt-based electrocatalysts for ORR in recent decades. According to our survey, no review article has provided a critical overview of innovative Pt-based electrocatalytic technology, morphological–activity relationships, shape-size dependence, and large-scale synthesis systems. Meanwhile, owning to the importance and rapid research progress, an updated review with very recent progress is also needed. This critical review offers an inclusive and systematic overview of the research trends and most recent advances in experimental and theoretical investigations, including nanomaterial selection, synthesis strategies, morphological characterization, and electrocatalytic activity. The enhancement of ORR activity and electrocatalyst stability is the perpetual chase for PEMFCs development. After introducing the electrochemistry of ORR using Pt-based electrocatalysts, we delve into innovative practical and theoretical strategies related to composition, particle size, shape, morphology, alloys, supporting materials, and single Pt-atom electrocatalysts. In addition, it explores their influence on activity and durability while emphasizing their relationship with the rational composition, size, and morphology of the Pt-based electrocatalysts.

2 ORR electrochemistry

This section introduces the fundamental electrochemistry of ORR when using Pt-based electrocatalysts, a deeply reported ORR mechanism. Although the ORR mechanism at the atomic level is complex, depending on the electrocatalysts used, the common electrochemical reduction reaction at the cathode for all the electrocatalysts involves four net coupled electron and proton transfers to molecular oxygen [28]. Various possible pathways exist for oxygen molecule electroreduction, including (i) two-electron reduction pathways to produce H_2O_2, (ii) directly four-electron reductions to H_2O in acidic solution and OH– in alkaline solution, (iii) two- and four-electron reduction "series" pathways, (iv) a combination of (ii) and (iii) called the "parallel" pathway, (v) the interactive pathway, which involves the diffusion of species from a "series" route into a "direct" route, (vi) the associative pathway, which involves the O_2 adsorption and direct electrons/protons transfer to it, leading to OOH dissociating into OH and O, and (vii) the dissociative pathway involves the breaking of the oxygen–oxygen covalent bond in the oxygen molecule, followed by the hydrogenation of atomic oxygen to H_2O and OH species [9].

For the Pt-based electrocatalysts, the specific ORR mechanisms have been proposed via either associative or dissociative adsorption of oxygen or both mechanisms operating at the same time. *In-situ* studies of $HOOH_{ad}$ and OOH_{ad} on commercial Pt/C reveal an associative mechanism in which the oxygen–oxygen bond-breaking only occurs at the peroxo level. OOH_{ad} exists at a high potential of 0.9 V, and $HOOH_{ad}$ is presented below the onset potential, as exhibited in Fig. 2(a). This supports the existence of a second, parallel ORR mechanism that excludes the same adsorbed intermediates and plays a significant role at the high potential [29].

Liu et al. [30] explained the ORR mechanism for the Pt-based electrocatalysts via theoretical calculations. Figure 2(b) demonstrates their proposed reaction pathways for completing ORR on the single Pt atom pyridinic N1-doped graphene (denoted g-P-N1-Pt1) electrocatalyst, illustrating the top and side views and bond lengths. In an acidic medium, the cycle (a) inset charts the free-energy chart for ORR on the g-P-N1-Pt1 electrode. Dong et al. [31] investigated *in situ* shell isolated nanoparticle enhanced Raman spectroscopy (ES-SHINERS) experiments and theoretical computations to elucidate the mechanism of ORR at the Pt(*hkl*) single crystal surface in the 0.1 M $HClO_4$ medium. The adsorbed oxygen molecules convert to HO_2* species through electron and proton transfer, dissociating to an O* and OH* on the adjoined Pt atom. The reactive OH* intermediates combine with hydrogen to produce H_2O molecule. A comprehensive schematic illustration how ORR goes on at a Pt(*hkl*) surface is revealed in Figs. 2(c) and 2(d), respectively. The protonation process takes part a prominent role in ascertaining the ORR mechanism and its activity.

3 Morphology controlled strategies

Morphology engineering plays a crucial role in regulating the electrocatalytic activity and stability. The electrocatalytic activity and stability of an electrocatalyst depend significantly on its morphology and arrangement of atoms, as well as surface area to volume ratio. Recent studies have confirmed that controlled morphology and structure of Pt and its alloy composites result in exceptionally high mass activity (MA) in the rotating disc electrode method. Furthermore, the morphology-controlled Pt has been found to enhance electrocatalyst durability. The nanoscale structures of morphology-controlled electrocatalysts include porous or aerogel forms of core–shell, nanowires (NWs), nanorods, nanotubes, nanoframes, and nanopolyhedron. It is noteworthy that the Pt-based electrocatalysts with controlled morphology are highly sensitive to morphology variations, and ORR is heavily dependent on the crystallographic stereochemistry of the Pt exterior. Several chemical and physical processes have been developed to engineer morphology-controlled Pt-based electrocatalysts, altering surface energies via temperature variation, reductants, seeds, and caping agents. The section presents an

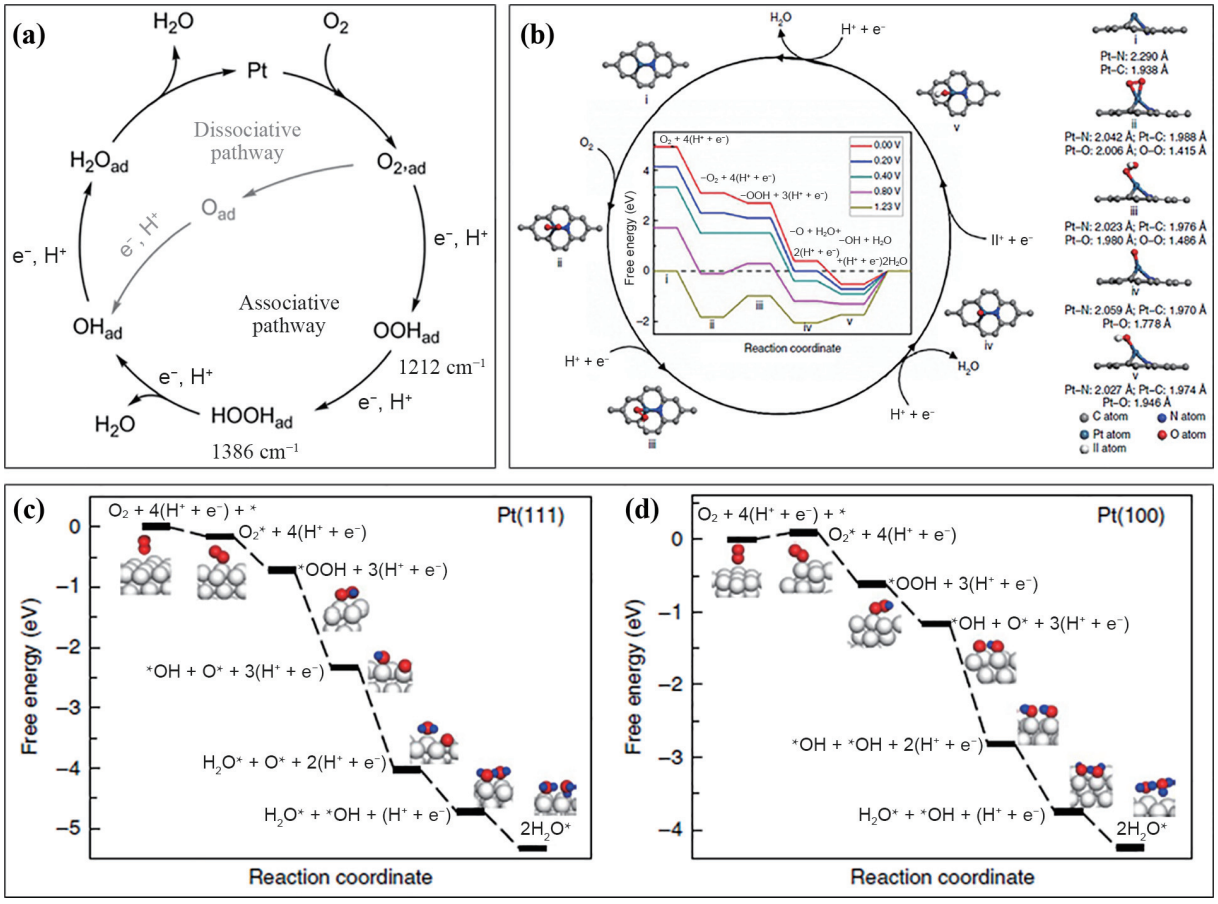

Figure 2 (a) ORR mechanism on Pt/C electrocatalyst in 0.1 mol/L perchloric acid medium. The associative pathway marks a superior impact at lower potentials. Reproduced with permission from Ref. [29], © 2018 Wiley-VCH Verlag GmbH & Co. KGaA, Weinheim. (b) The proposed ORR pathway on the optimized g-P-N1-Pt1 electrocatalyst. Free energy graph (inside cycle) for the g-P-N1-Pt1 electrocatalyst in an acidic solution. Reproduced with permission from Ref. [30], © Liu, J. et al. 2017. Various intermediates at (c) Pt(111) surface and (d) Pt(100) surface. The white sphere represents Pt; the red sphere denotes oxygen; and the blue sphere represents hydrogen. The key dissimilarity between ((c) and (d)) is the fourth phase. In case of (c), $3(H^+ + e^-) + O^* + OH^* \rightarrow 2(H^+ + e^-) + O^* + H_2O^*$, and in case of (d), $3(H^+ + e^-) + O^* + OH^* \rightarrow 2(H^+ + e^-) + OH^* + OH^*$. Reproduced with permission from Ref. [31], © Dong, J. C. et al. 2018, under exclusive licence to Springer Nature Limited.

overview of the innovative areas of morphology-controlled Pt-based electrocatalysts, along with the corresponding improvements in activity and durability, as summarized in Table 1.

3.1 Nanocubes/nanoframes

Nanoframes and nanocubes hold great promise as a novel group of electrocatalysts due to their unique morphologies offering a high proportion of effective surfaces and reducing the need for costly Pt loading. Three-dimensional (3D) molecular accessibility on interior and exterior surfaces further enhances their potential for catalytic applications. An innovative approach employed by Park et al. [33] implicated the selective deposition of Pt atoms on the corners and edges of palladium nanocube templates, producing Pd@Pt core frame nanocube (Fig. 3(a)). Optimization of kinetics for Pt surface diffusion and deposition allowed for the selective site deposition of Pt on Pd nanocubes, and chemical etching selectively detached the Pd cores to create Pt cubic nanoframes that were thoroughly dispersed on carbon support to form the Pt nanocube nanoframe/C electrocatalyst. The as-prepared electrocatalyst exhibited high initial mass ORR activity and stability due to its distinctive morphology, which prevented particle detachment and aggregation.

Similarly, Kwon et al. [34] used accurate kinetic control to synthesize very porous hierarchical multiframe electrocatalysts using dendrite-implanted Pt-Ni multiframes supported on carbon (Figs. 3(b)–3(d)). The multiframed structure promoted the interior access of chemicals, while the interconnectivity between multiframes contributed to its stability under catalysis. The extensive use of nickel as a space-filler promoted the Pt-Ni dendrites aggregation and allowed for rapid Pt atoms movement to the surface, following in a multiframe structure that exhibited 30 times higher MA than commercial Pt/C. Finally, the novel Pt multicubes synthesized by Ma et al. [46] surrounded via (100) facets containing high-index facets at the small junction area between neighboring cubic constituents exhibited remarkable ORR activity due to the low resistance by the flat surface and active sites via high-index facets as confirmed in the high-resolution transmission electron microscopy (HRTEM) images (Figs. 3(e) and 3(f)). Owing to enhanced electron transport, nanowires with corrosion resistance and outstanding stability are regarded a distinctive class of Pt-based electrocatalysts.

3.2 Core–shell structure

Core–shell electrocatalysts with Pt shells and economical materials have attracted significant research attention in NP engineering. Controlling the atomic arrangement and thickness of Pt rich shell is the key parameter of Pt-based electrocatalysts [47]. The core–shell morphology enables the efficient utilization of Pt NPs by coating them with a narrow layer of Pt atoms shell around a cheap core such as Pd NPs. Chen and co-workers [48] investigated the morphological advancement of the PtML@Pd/C core–shell electrocatalyst. They found that the PtML@Pd/C electrocatalyst presented a volcano-like profile during a stability

Table 1 Morphology controlled electrocatalysts for the recently reported ORR with high activity and stability in 0.1 mol/L $HClO_4$ solution[a]

Electrocatalyst	Morphology	SA ($mA \cdot cm^{-2}$)	MA ($A \cdot mg_{pt}^{-1}$)	ECSA ($m^2 \cdot g^{-1}$)
PtIr DTPs [32]	Tripods	1.83	0.77	42.1
Pd@Pt [33]	Core–frame nanocubes	1.17	0.82	85
Pt-Ni [34]	Multiframes	7.06	1.51	73.4
Ir@Pt [35]	Core–shell	1.28	0.42	37
PtPb/Pt [36]	Core–shell nanoplate	7.8	4.3	55
Mo-Pt_3Ni [37]	Octahedral	10.3	6.98	67.5
Pd@Pt [38]	Core–shell octahedra	0.73	0.48	79.0
$Pt_{1.5}$Ni-BNSs [39]	One-dimensional bunched nanocages	2.20	1.02	68.2
PtNi alloy [40]	Jagged nanowires	11.5	13.6	118
Pt-Pd SBCNCs [41]	Symmetry-broken concave nanocube	1.93	0.87	45.2
Pt-Co ND-NF [42]	Nanodendrite in nanoframe	2.624	0.939	35.6
PtCo NRAs [43]	Nanorod assemblies	1.854	0.914	48.32
Pt_1Pd_1/C [44]	Nanodendrite	1.33	1.164	53.8
PtPdCu HCRDs [45]	Hexapod concave rhombic dodecahedrons	2.20	1.17	53.3

[a]SA: specific activity at 0.9 V vs. RHE, MA: mass activity at 0.9 V vs. RHE.

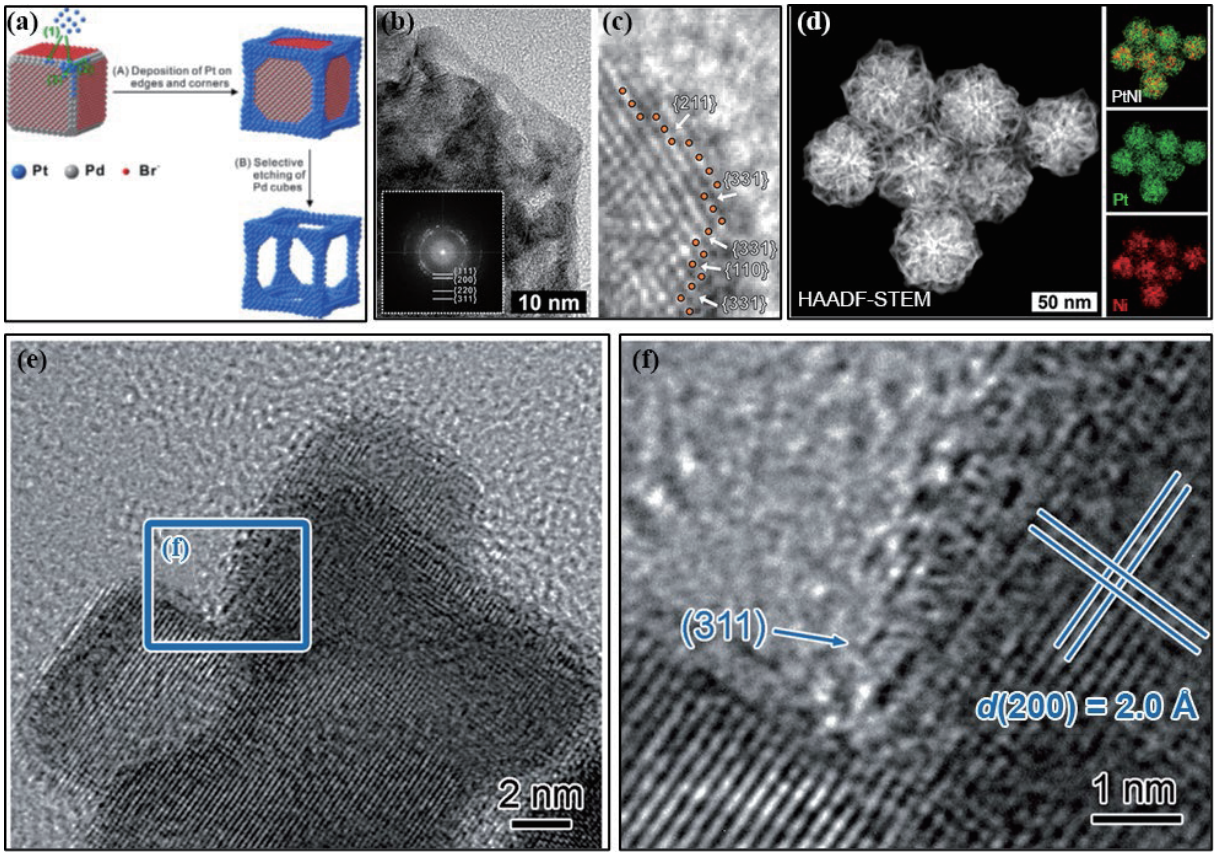

Figure 3 (a) Schematic shows the synthesis of a Pt cubic nanoframe. Reproduced with permission from Ref. [33], © Wiley-VCH Verlag GmbH & Co. KGaA, Weinheim 2016. (b) TEM image of the optimized Pt-Ni multiframes. (The FFT pattern is shown in inset of (b)). (c) The surface atomic steps and kink sites (HRTEM images) of PtNi composite. (d) HAADFSTEM and elements plotting images of the PtNi composite. Reproduced with permission from Ref. [34], © American Chemical Society 2018. (e) and (f) The HRTEM images of a Pt multicubes. Reproduced with permission from Ref. [46], © WILEY-VCH Verlag GmbH & Co. KGaA, Weinheim 2015.

upto 100,000 cycles. The activity of the core–shell electrocatalyst increased until about 20,000 cycles. The newly formed Pt monolayers settled all atoms on the 4-fold and 3-fold hollow sites of the Pd surface and reduced into a whole coverage on the Pd core, which improved the dissociative adsorption of oxygen. Zhang's group [49] developed a gram-batch strategy for preparing Pd@Pt/C core–shell electrocatalysts for ORR using three different pathways: (i) reduction via a negative charge on palladium surface, (ii) chemical reduction via citric acid, and (iii) galvanic displacement reaction between palladium and Pt. The citric acid was found to be instrumental in the morphology controlling of the Pt shell. Pd@Pt/C core–shell electrocatalysts prepared via citric acid exhibited four-fold higher MA and outstanding stability upon potential cycling. Considering their ease of synthesis and excellent electrochemical performance, Pd@Pt/C core–shell electrocatalyst is believed to be the best choice for PEMFCs.

Particle sintering behaviors and morphological ordering are important factors for the improvement of Pt-based intermetallic electrocatalysts. Wang and co-workers. [50] synthesized three carbon-supported $PtCo_3$, $PtNi_3$, and $PtFe_3$ electrocatalysts through thermal annealing (Fig. 4(a)), with the ordered $PtCo_3$ catalyst exhibiting the highest ORR activity and stability due to the uniformly thin Pt shells and utmost Co content in the ordered intermetallic core after 10,000 cycles. Li et al. [51] confirmed that the intermetallic $L1_0$-FePt/Pt core–shell, with a thin, smooth Pt shell compressed because of epitaxial binding with $L1_0$-FePt core, is chemically stable for ORR (Fig. 4(b)). The as-prepared $L1_0$-FePt/Pt electrocatalyst exhibited excellent MA of 0.7 $A{\cdot}mgpt^{-1}$ at 0.9 V and outstanding stability. This concept presents a strategy for engineering of $L1_0$-CoPt/Pt and $L1_0$-CoNiPt/Pt as an exceptional electrocatalyst for PEMFCs, where compressive surface strains are crucial to increase ORR activity in core–shell metal/Pt electrocatalysts. Bu and co-workers [36] synthesized Pt-Pb/Pt core–shell nanoplate electrocatalysts, which showed large biaxial strains and high specific activity (SA) of 7.8 $mA{\cdot}cm^{-2}$ and high MA of 4.3 $A{\cdot}mgpt^{-1}$ at 0.9 V vs. reversible hydrogen electrode (RHE), with scanning transmission electron microscopy (STEM)-electron energy-loss spectroscopy confirming the Pt and Pb distribution at the nanoplates (Fig. 4(c)) where the individual Pt and Pb metals, and combined images showed the existence of a Pt edge layer around the PtPb core (Fig. 4(d)). Density functional theory (DFT) calculations confirm that the Pt(110) facets and edge-Pt optimize the Pt–O bond strength. The PtPb/Pt nanoplates, with an intermetallic core and uniform 4-layers of Pt shell, exhibit high endurance with negligible performance deterioration and no observable changes in composition and structure after 50,000 cycles. Strickler's group [35] synthesized Ir@Pt core–shell catalysts with different compositions through a scalable one-step polyol synthesis approach (Fig. 4(e)) and identified the most active electrocatalyst as the 3.4 nm Ir@Pt NPs in a core–shell, exhibiting remarkable ORR performance with MA of 0.35 $A{\cdot}mgpt^{-1}$ and SA of 0.90 $mA{\cdot}cm^{-2}$, as well as better stability with increasing MA of 0.42 $A{\cdot}mgpt^{-1}$ and SA of 1.28 $mA{\cdot}cm^{-2}$ after 10,000 cycles (Fig. 4(f)). Improvement of MA for the Ir@Pt electrocatalyst can be achieved through various measures such as increasing NP dispersion, improving shell coating homogeny, reducing shell thickness, and optimizing NPs morphology.

Based on the above discussion, we concluded that designing morphology-controlled Pt-based core–shell architectures is a promising approach to maximize the usage of Pt utilization while maintaining remarkable ORR activity. In addition, a thick-shell strategy is proposed to enhance the durability of the core–shell architectures via thwarting the core from dissolution.

3.3 Nanowires

Nanostructures with one dimension, including nanorods and nanowires, have gained significant attention due to their peculiar, anisotropic morphology that can benefit the ORR process. The NWs, nanorods, and nanotubes are characterized by a large

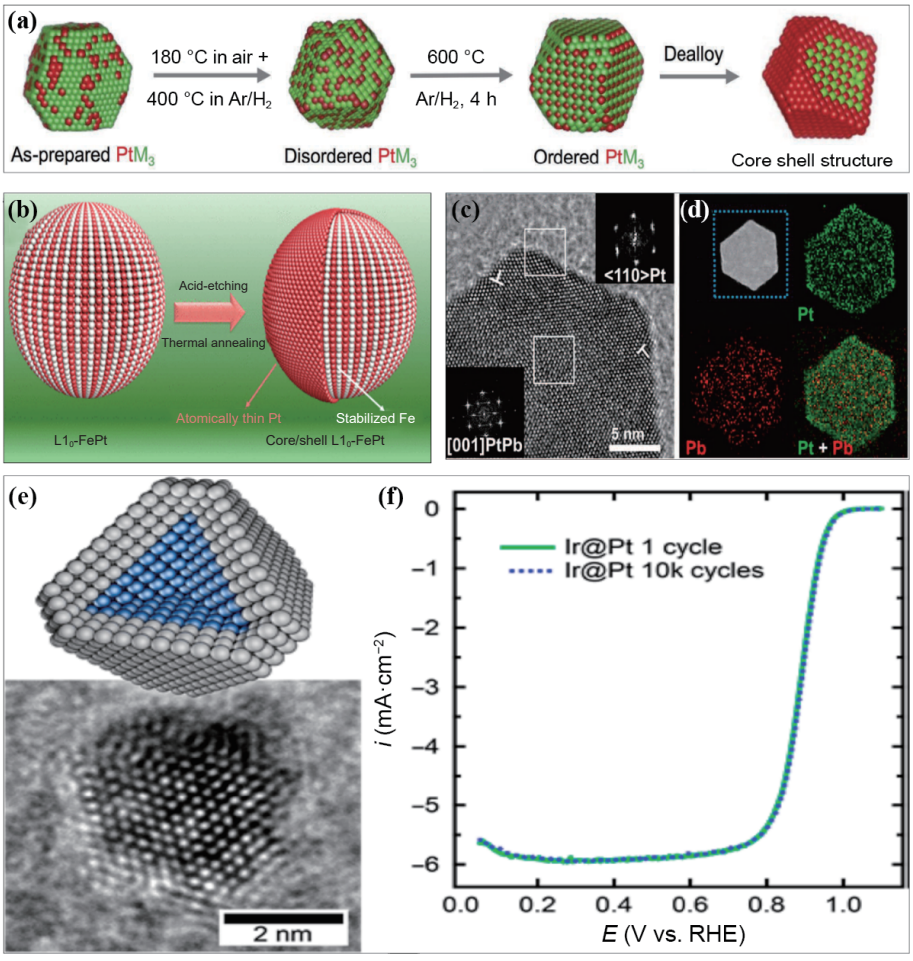

Figure 4 (a) The synthetic sketch of structurally ordered and disordered low-Pt (PtM_3, M = Co, Ni, and Fe) intermetallic electrocatalysts. Reproduced with permission from Ref. [50], © WILEY-VCH Verlag GmbH & Co. KGaA, Weinheim 2019. (b) Schematic illustration of core–shell L10-FePt/Pt NPs. Reproduced with permission from Ref. [51], © American Chemical Society 2018. (c) HRTEM of one PtPb single hexagonal nanoplate. The insets of (c) show the FFT patterns and (d) HAADFSTEM and elemental mapping images of Pt, Pd, and PtPb. Reproduced with permission from Ref. [36], © American Association for the Advancement of Science 2016. (e) HRTEM images of Ir@Pt core–shell electrocatalysts. (f) Electrochemical stability of commercial Ir@Pt core–shell electrocatalyst. Reproduced with permission from Ref. [35], © American Chemical Society 2016.

contact area crucial for stable Pt anchoring on the carbon support. Enhanced stability requires high surface area, good conductivity, flexibility, and anisotropic morphology.

Hoque et al. [52] observed that Pt NWs containing multiple single-crystalline NPs existed along the (111) crystallographic direction showed remarkable activity and durability for ORR when combined with sulfur-doped graphene (SG). Following 3000 cycles, the PtNWs/SG maintains 58% of its initial electrochemically active surface area (ECSA), outperforming PtNWs/G and commercial Pt/C, which retained only 28% and 1%, respectively. Chen and co-workers [53] performed multiscale atomic simulations of jagged Ni_7Pt_3 NWs, which displayed exceptional ORR activity. According to DFT simulations, 14.4% of the NW surface sites were barrierless for $H_2O_{ads} + O_{ads} \rightarrow 2OH_{ads}$, which are considered the rate-determining step. This is caused by the concave surfaces of many sites, which push the OH bond of H_2O_{ads} towards O_{ads}, ultimately reducing the barrier. The J-PtNWs were found to yield enhanced performance relative to Pt(111) due to the undercoordinated rhombus-rich surface configurations and highly-stressed jagged-P NWs (Fig. 5(a)). Li et al. [40] reported that Pt/NiO core–shell NWs transformed into PtNi alloy NWs via thermal annealing, which was subsequently converted into jagged-Pt NWs through an electrochemical dealloying process, as illustrated in Fig. 5(b). The jagged-Pt NWs exhibited a SA of 11.5 $mA{\cdot}cm^{-2}$ and ECSA of 118 $m^2{\cdot}g^{-1}$, leading to a MA of 13.6 $A{\cdot}mgpt^{-1}$. Ma and co-workers [54] studied the synthesis of Pt NW network electrocatalysts through a solid-state reaction, yielding free-standing Pt NWs with up to 5.1 times MA and only a 2.6% loss after 10,000 cycles, as well as 8.5 times SA compared to commercial Pt/C. Additionally, several substrate materials were employed to support Pt-based NWs with a wet impregnation technique.

Jin et al. [55] designed a controllable composition anisotropic mesoporous Pt@Pt-skin Pt_3Ni core–shell framework NWs exhibited in Fig. 5(c). The as-prepared electrocatalyst has atomic jagged Pt NWs core with a mesoporous Pt-skin Pt_3Ni framework shell, possessed remarkable activity and durability.

3.4 Dendritic nanocrystals

Nanocrystals with dendritic morphology possess high surface area and are considered attractive electrocatalysts for ORR. A facile one-step synthesis strategy for controlled engineering of PtIr dendritic surface tripods (PtIr DTPs) has been reported by Lu et al. [32] The novel PtIr DTPs electrocatalyst has demonstrated exceptional electrocatalytic activity and stability. The developed innovative strategy for synthesizing a dendritic Pt-based tripod is viable, where composition and morphology are critical factors contributing to the remarkable electrocatalytic activity and stability. The hierarchical dendritic nanostructure of PtIr DTPs imparts many functional sites accessible at the surface. Additionally, a large number of inner cavities are distributed throughout the dendritic morphology, with spatially divided branches, which promote the migration of reactive species throughout the entire surface. This protects active electrocatalytic sites from blocking by intermediates. Moreover, the strain and electronic effects produced by the bimetallic composition intensify the adsorption of oxygen, facilitating oxygen-oxygen splitting at very low voltage with a high tolerance for intermediates species such as H_2O_2, O_2^-, and O_2^{2-}.

4 Supporter synergistic effect strategy

Currently, commercial carbon is the most widely used support for Pt catalyst. However, when exposed to oxygen, carbon corrosion can occur at high electrode potentials, causing Pt NPs to separate from the carbon and leading to a loss in activity. Additionally, the weak interaction between Pt NPs and carbon support can result in migration and aggregation of Pt NPs, which can contribute to a reduction in the active surface area, particularly over long-term operations such as those experienced in automobile applications. To address these critical issues, scientists have focused on developing high graphitic carbon materials. For example, carbon nanotubes (CNTs), carbon nanofibers, and graphene, intend to improve the relationship between Pt NPs and support. Indeed, numerous Pt-based electrocatalysts have recently been synthesized, and Table 2 provides an overview of the most commonly used supports for ORR.

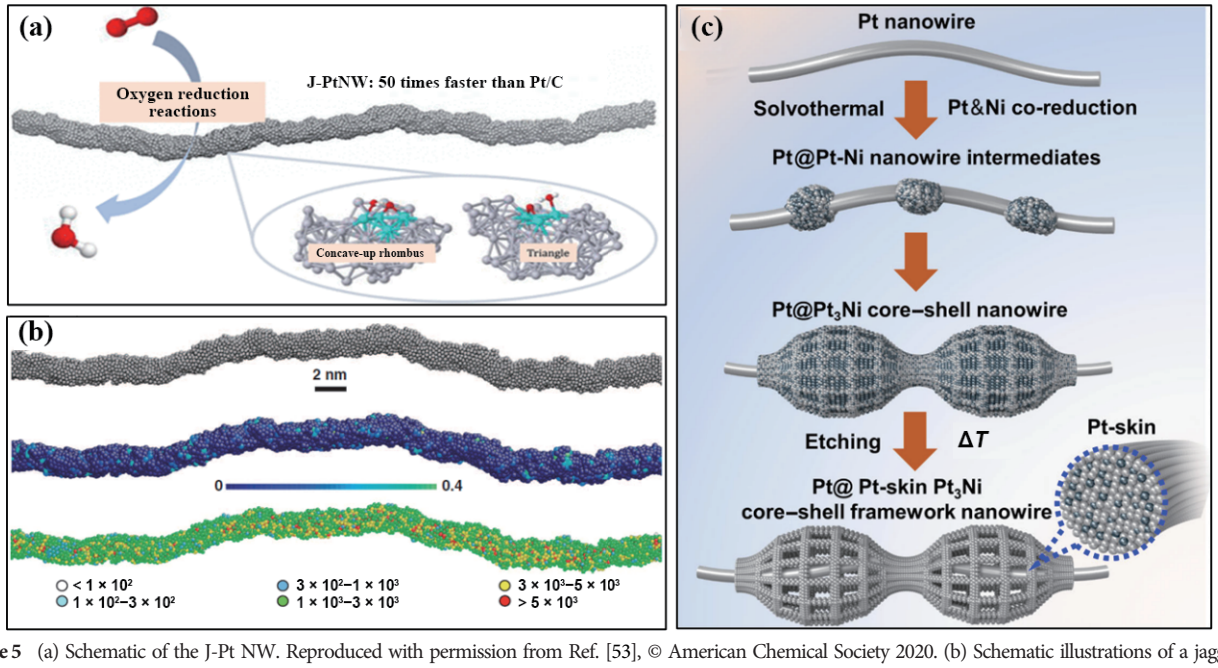

Figure 5 (a) Schematic of the J-Pt NW. Reproduced with permission from Ref. [53], © American Chemical Society 2020. (b) Schematic illustrations of a jagged-Pt NW created via reactive molecular dynamics simulations, with an average diameter and length of ~ 2.2 and 46 nm, respectively. The colored atoms of jagged-Pt NW illustrate the five-fold index and the atomic stress distribution. Reproduced with permission from Ref. [40], © American Association for the Advancement of Science 2016. (c) Schematic of the synthesis of mesoporous Pt@Pt-skin Pt_3Ni core–shell framework NW (ΔT denoted annealing treatment). Reproduced with permission from Ref. [55], © Jin, H. et al. 2023.

Table 2 Comparative analysis of the ORR activity of several most common support Pt-based electrocatalysts

Electrocatalyst	Supporting materials	SA ($mA·cm^{-2}$)	MA ($A·mgpt^{-1}$)	ECSA ($m^2·g^{-1}$)
Pt/BNG [56]	B, N dual-doped graphene sheets	0.350	0.213	63.14
Pt/Co-NST [57]	Cobalt encapsulated in N, S co-doped carbon nanotube	723.93	0.508	70.23
$Pt/Ti_{0.8}Co_{0.2}O_2$ NTAs [58]	Binary titanium cobalt oxide nanotubes	0.96	0.53	57.4
Pt/rGO [59]	Reduced graphene oxide	0.665	0.092	14.0
Pt/40 wt.%-SnO_2-C [60]	SnO_2-C nanocomposites	0.30	0.066	69
$Pt/Ti_{0.9}Ni_{0.1}N$ NTs [61]	Titanium nitride nanotubes	1.3	0.78	59.7
PtNW/SGs-2 [62]	Sulfur doped graphene	0.662	0.182	28.5
Pt NPs encapsulated in zirconiananocage [63]	Zirconia nanocage	—	0.28	—
Pt/TiN [64]	3D titanium nitride	1.06	0.65	61
Co_3O_4-Pt @3DG-2 [65]	3D graphene	2.17	1.018	46.89
Pt/CNT–$Ti_3C_2T_x$ (1:1) [66]	MXene ($Ti_3C_2T_x$) hybrid with a CNT	0.259	0.163	63.0
Pt/TiO_2 [67]	TiO_2	1.134	0.083	7.23
PtCo/CoNC NR [68]	Co-N-C nanorods	1.4	0.577	44.3

4.1 Carbon-based supporter strategy

Carbon black and graphene are the two most used supporting materials for Pt NPs. Carbon black is desirable due to its low price, different surface areas, surface functionality, and good conductivity, making it an excellent support material [69]. On the other hand, graphene is a thin nanosheet composed of C-atoms that are covalently linked in a hexagonal shape. It offers outstanding electrochemical stability, high electronic conductivity, and a large surface area. Furthermore, graphene also undergoes various modifications, such as 2D and 3D graphene, reduced graphene, and graphene quantum dots, all of which make them the most suitable support material for Pt NPs in different applications. The graphene shell plays role to reduce the Pt–OH adsorption or other intermediates. According to a recent study of Park et al. [70], the graphene shell plays a promising role to weaken the Pt–OH adsorption or other intermediates.

Ma et al. [71] utilized the photoreduction process to produce Pt NPs of varying sizes loaded on N-doped carbon nanotubes (CNTs). The researchers found that the Pt electrocatalyst with 3 nm size exhibited the best ORR with the MA being 16 times compared to Pt/C in alkaline medium. Conversely, Zhu's group [72] synthesized Pt NPs on boron and nitrogen-doped graphene sheets (BNG) and boron and nitrogen codoped carbon nanofibers (BNCNF) for ORR. Their research indicated that compared to single-doped carbon and commercial graphene support, BNCNF and BNG offer a greater number of active sites and defects (Fig. 6(a)). Pt NPs with the optimal diameter (2–3 nm) were highly dispersed across the supports, and BNCNF and BNG interacted strongly with Pt, preventing the aggregation of Pt NPs during potential cycling tests (as seen in Figs. 6(b) and 6(c)). The researchers hypothesized that electron transportation from the BNCNF and BNG to the Pt NPs promotes ORR via lowering the oxygen adsorption barrier. Lastly, Hoque et al. [62] investigated PtNW/S-doped graphene employing a combination of experimental and computational strategy. The researchers observed that the quantity of sulfur substantially influenced the ORR kinetics of NW electrocatalysts since the presence of sulfur in S-doped graphene increased the number of graphene sheets as the sulfur content increased. The less graphitic nature of sulfur-doped graphene was highlighted by the decrease in the ratio of sp^2 and sp^3 carbons. The electrocatalytic performance of PtNW/SG-2 is optimized, with a MA of 182 $mA·mgpt^{-1}$ and SA of 662 $\mu A·cm^{-2}$. Lin et al. [73] utilized sol-gel techniques to prepare electron acceptor N-doped carbon nanosheets with high graphitization for optimizing the electronic structure of Pt particles (Fig. 6(d)). The metal–support interaction causes a reduction in the electron density on the surface of Pt atoms. Moreover, the metal–support effect lowers the Pt-oxygen dipole effect, preventing Pt dissolution and thus enhancing catalytic stability. The as-prepared catalyst has a Pt dissolution rate of only 1/18 of commercial Pt/C in an acidic electrolyte. Furthermore, by analyzing the dissolution of Pt atoms and the desorption process, it was observed that the electrocatalyst exhibits a larger potential barrier during the initial relaxation process, contributing to better stability. DFT simulations suggest that the electrons are transferred from Pt to the carbon substrate, reducing the electron cloud density of Pt. This reduced density, in turn, makes it challenging for Pt to transfer electrons to oxygen on the surface, thereby weakening the Pt–O dipole effect on the surface.

Based on the above discussion, we concluded that carbon-based supporting materials play a key role to suppress the degradation of Pt electrocatalyst in the electrochemical ORR.

4.2 Non-carbon supporter strategy

Various non-carbon supporting materials have been explored for their strong metal–support interaction and high corrosion resistance to provide robust support for Pt NPs. These materials include metal oxides, nitrides, carbides, borides, as well as zirconia (ZrO_2), among others. To stabilize Pt encapsulated in ZrO_2 nanocages, Cheng's team [63] presented a straightforward approach that utilizes area-selective atomic layer deposition. The encapsulated Pt NPs demonstrated a remarkable ability to resist migration and agglomeration, rendering enhanced activity and stability toward the ORR in acidic solution. A range of applicable metal oxides with optimum electrical conductivity is readily available, with doping strategies widely employed to facilitate electron conductivity. In a study by Zhao and colleagues [74], the activity of Pt loaded on tin-doped indium oxide (ITO) was evaluated in alkaline solution. In terms of performance, the obtained results demonstrated that the Pt@ITO composite outperformed Pt/C. Specifically, the SA and MA of Pt@ITO electrocatalyst are around 2.5 times compared to Pt/C. After 300 cycles in oxygen saturated alkaline solution, a loss of around 17.4% in electrochemical surface area for Pt@ITO electrocatalyst is favorably compared to commercial Pt/C (37.5%). Several researchers have investigated using co-doped TiO_2 as a support material for Pt NPs. Hsieh et al. [75] synthesized Pt NPs supported on TiO_2 co-doped with nitrogen as an anion and niobium or tungsten as a cation. This approach led to higher electron

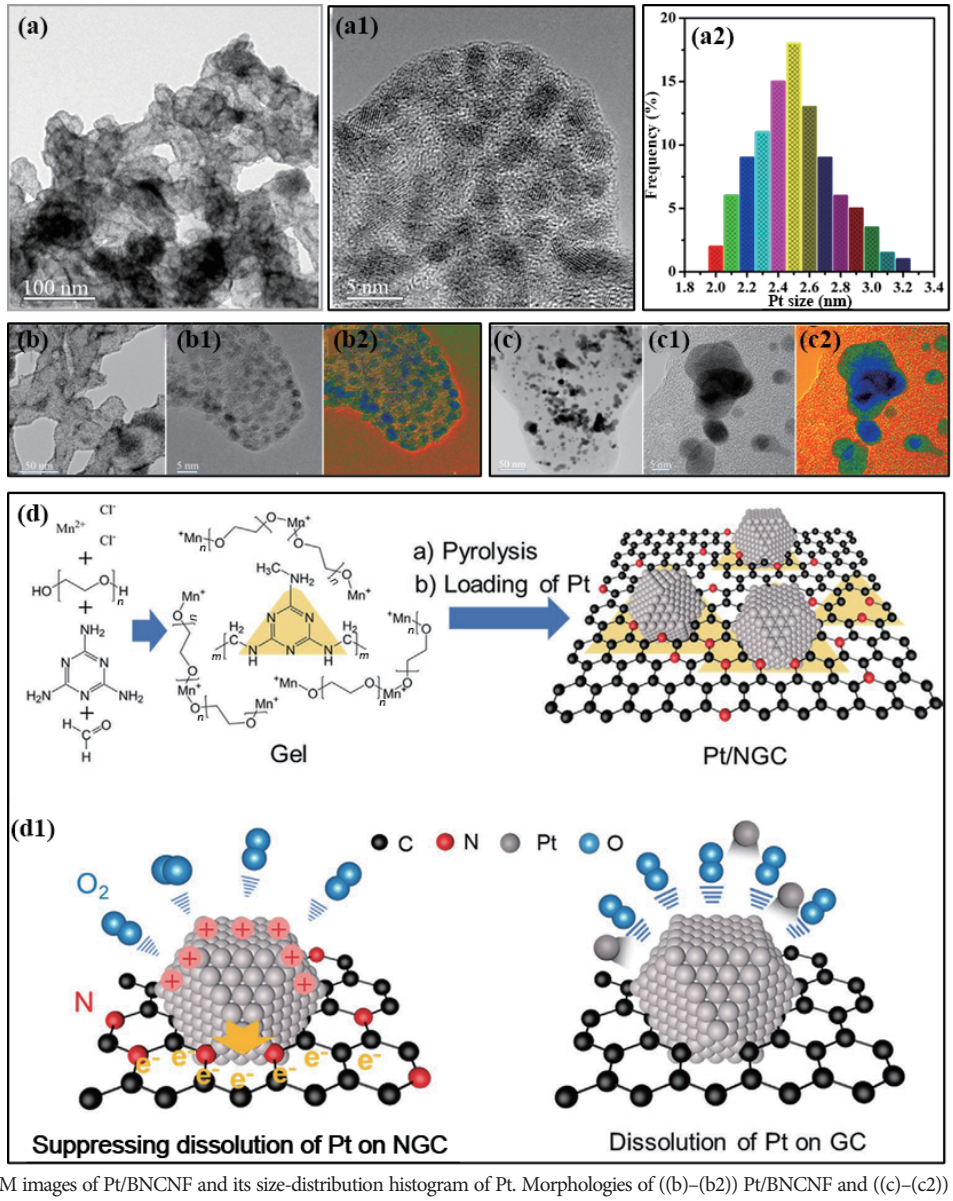

Figure 6 (a)–(a2) TEM images of Pt/BNCNF and its size-distribution histogram of Pt. Morphologies of ((b)–(b2)) Pt/BNCNF and ((c)–(c2)) Pt/C after cycling tests. Reproduced with permission from Ref. [72], © The Royal Society of Chemistry 2018. (d) The synthesis of Pt/NGC, and (d1) dissolution of Pt impeded via NGC weakening the Pt–O interaction. Reproduced with permission from Ref. [73], © Wiley-VCH GmbH 2021.

conductivity, resulting in improved electrochemical performance. The co-doping also altered the electronic state of Pt atoms, leading to promising active and stable catalysts. Defect formation influenced the interactions between Pt and the doped TiO_2 support material. Another study by Zheng et al. [64] focused on synthesizing 3D TiN with porous architectures of interconnected NWs assemblies. The 3D morphology of the support provided numerous active sites, facilitating high electron transfer and enhancing the contact between the electrocatalyst and electrolyte. Yu and coworkers [58] developed a facile one-pot approach for synthesizing binary titanium cobalt oxides ($Ti_{0.8}Co_{0.2}O_2$) as a support for Pt NPs. The $Ti_{0.8}Co_{0.2}O_2$ nanosheet assembly served as a strong support, driving efficient dispersion of Pt NPs and acting as a co-catalyst to enhance the ORR activity. Using the photo-deposition method, Estudillo-Wong et al. [76] synthesized Pt NPs loaded on yttrium-doped TiO_2-C (Y:TiO_2-C) composite. The Y:TiO_2-C composite support improved the stability of Pt/Y:TiO_2-C catalyst and exhibited excellent ORR activity. While each support material has advantages and limitations, combining different materials in hybrid structures can result in synergistic effects that can overcome these drawbacks.

5 Alloying strategies

Based on Pt-Alloy's strategy, alloying Pt with different metals provides a clear advantage over pure Pt electrocatalysts. A high MA may be exhibited by combining another precious or non-precious metal with reduced Pt loading. The electronic modifications induced by the interaction between the two metals contribute to excellent ORR activity [21]. Successful strategies for increasing electrocatalytic ORR include Pt alloying with transition metals (TMs). Moreover, the Pt alloy effect is linked to three factors, including ensemble effect, electronic effect, and strain effect [24].

5.1 Bimetallic alloys

Combining Pt with abundant and less expensive transition metals, such as nickel (Ni), copper (Cu), iron (Fe), or cobalt (Co) is a promising approach to reduce the utilization amount of Pt and the cost of PEMFCs while enhancing their ORR activity. The ORR kinetic on the Pt surface is hindered by the strong binding energy of adsorbed oxygen species that need to be removed from the catalyst surface. The addition of metal to Pt can weaken the adsorption of oxygen species on the surface of the electrocatalyst

via strain and ligand effects, thus enhancing the ORR performance. In recent years, several Pt bimetallic electrocatalysts (Table 3) have been developed and tested for ORR.

In order to link electrocatalytic activity with alloys, Colic et al. [87] reviewed literature data and concluded that model single crystal Pt-alloys exhibit high activity for ORR. PtCo alloys have been widely studied in terms of particle sizes, compositions, and synthesis parameters, and Zhang et al. [88] reported a locally distributed atomic PtCo N-carbon (A-PtCo-NC) electrocatalyst with excellent activity and stability for ORR. DFT calculations confirmed that the synergistic effect of Pt and Co in the specific coordination construction resulted in d-orbital shift and charge redistribution, leading to the excellent electrocatalytic performance of A-PtCo-NC. Wang's group [89] developed a facile one-step strategy for synthesizing Pt–Co alloy concave nanocubes, which exhibited SA of 2.34 $mA·cm^{-2}$ and MA of 0.26 $A·mgpt^{-1}$, higher than those of Pt/C catalysts. Moreover, after 5000 cycles, the PtCo/C electrocatalyst maintained a higher MA compared to commercial Pt/C.

PtNi alloys are also promising candidates for ORR. Various alloy composition strategies have been explored to boost electrochemical activity and stability. Mezzavilla and co-workers [90] studied the bimetallic family of PtNi NPs encapsulated in hollow graphitic spheres, as illustrated in Fig. 7(a). Due to their remarkable SA and ECSA, Pt_3Ni, PtNi, and $PtNi_3$ exhibited MA of 2, 3, and 3.5 times higher, respectively, compared to Pt NPs of similar particle size distribution, as shown in Fig. 7(b). This research determines the potential of confined space alloying as a novel approach for developing efficient ORR electrocatalysts.

PtCu alloys have exhibited noteworthy activity and stability towards ORR, as reported by Coleman et al. [91]. They studied the kinetics of ORR on PtCu/C catalyst, which was found to have reduced surface affinity for OH_{ads} than Pt/C catalysts (Fig. 7(c)). Based on the study of OH_{ads}, the researchers concluded that PtCu/C has an initial as well as changing rate of the OH_{ads} coverage, highlighting the production of an irreversible oxide film. Furthermore, the reversible OH_{ads} coverage per unit of potential change (Fig. 7(d)) was revealed to be high for commercial Pt/C in comparison to PtCu/C in a 0.1 mol/L $HClO_4$ medium, revealing a higher affinity of Pt/C towards OH_{ads} compared to PtCu/C. Therefore, the authors suggest that Pt-based electrocatalysts display weaker Pt–OH or Pt–O bonding, leading to a remarkable increase in the ORR activity.

The use of chemically ordered PtFe alloys has resulted in remarkable ORR activity. For instance, Jung et al. [79] developed Pt_3Fe/C electrocatalysts that exhibited a four-fold higher MA of 0.454 $A·mgpt^{-1}$ compared to Pt/C, thanks to the outstanding stability of the intermetallic phase. Additionally, galvanic replacement reaction has proven to be a valuable and efficient method for developing Pt-alloy catalysts. Bordley's group [92] conducted experiments on the SA of four Pt-Ag alloy nanocage catalysts and revealed the dependence of SA on Pt content. The results showed that incorporating Pt into silver nanocubes (Pt-Ag nanocage catalysts) enhanced the specific current density by at least a factor of 1.5 compared to pure Pt. Interestingly, the nanocages with the low Pt content showed the highest activity among all Pt-Ag nanocage catalysts tested. Furthermore, Yavuz and co-workers [93] investigated the ORR activity of Mo oxide and Pt NPs modified electrode and found that electrodeposition of Mo oxide and Pt NPs on a glassy carbon (GC) electrode substantially increased the cathodic peak current and potential. This remarkable activity can be ascribed to the hypo-hyper d combinations between metal and metal oxide.

Synthesis of carbon-supported Au-decorated Pt NPs by Wang et al. [94] has highlighted several noteworthy benefits over Pt-based catalysts. First, the size of Pt NPs can be controlled to be similar. Second, the position of Au on Pt is random, preventing changes to the exposure of the crystal facets of all Pt clusters. Third, the impregnated Au has a negligible effect on the lattice strain of Pt. These features have led to the selection of Au-decorated Pt NPs to regulate the role of electron charge transfer in the ORR performance. The exclusion of structural factors such as particle size, lattice strain, and crystal facet allows for a focus solely on electronic interactions between Au and Pt in relation to the ORR performance. In a separate study, Pt–Pd/C alloy electrocatalyst synthesized by Wang and co-workers [95] via the room-temperature electron reduction process featured mainly (111) facets, resulting in weaker oxygen-binding and boosting oxygen–oxygen bond breaking and OH desorption. The MA of the as-prepared Pt1Pd1/C electrocatalyst was approximately four times that of the commercial Pt/C and demonstrated 96.5% retention of the MA after 10,000 cycles, highlighting exceptional stability.

Rh-doped Pt NWs/C electrocatalysts developed by Huang et al. [96] demonstrated exceptional ORR in terms of activity and stability. Compared to Pt/C, the Rh-doped Pt NWs@C electrocatalyst exhibited remarkable improvements in MA and SA by 7.8- and 5.4-fold, respectively. When subjected to 10,000 cycles, Rh-doped Pt NWs@C showed only a 9.2% drop in MA, whereas the commercial Pt/C exhibited a significant 72.3% decrease. The excellent stability is attributed to the large vacancy formation energy of the Pt atoms in Rh-doped Pt NWs. Moreover, Pt alloys

Table 3 Comparative review of the ORR of bimetallic Pt electrocatalysts in 0.1 M $HClO_4$

Electrocatalyst	SA ($mA·cm^{-2}$)	MA ($A·mgpt^{-1}$)	ECSA ($m^2·g^{-1}$)
Pt_3Co NWs/C [77]	7.12	3.71	52.1
Pt_3Co/C [78]	1.00	0.539	53.8
Pt_3Fe/C [79]	1.4	0.454	37.6
PtxY600h5 [80]	1.57	0.586	32.9
$Pt_{59}Ni_{41}$/C [81]	0.61	0.330	54
NiPt-300 2D nanoframe [82]	5.8	0.29	5.3
$Pt_{78}Pd_22$/C NWs [83]	1.04	0.92	70
Pt_1Pd_1/C [44]	1.33	1.164	53.8
Pt-Pd SBCNCs [41]	1.93	0.87	45.2
PtAu/CB600[84]	0.45	0.41@0.85 V	91.22
PtAg-4 NTs/C [85]	1.13	0.688	60.4
$Pt_{76}Cu_{24}$ [86]	1.273	0.466	36.6

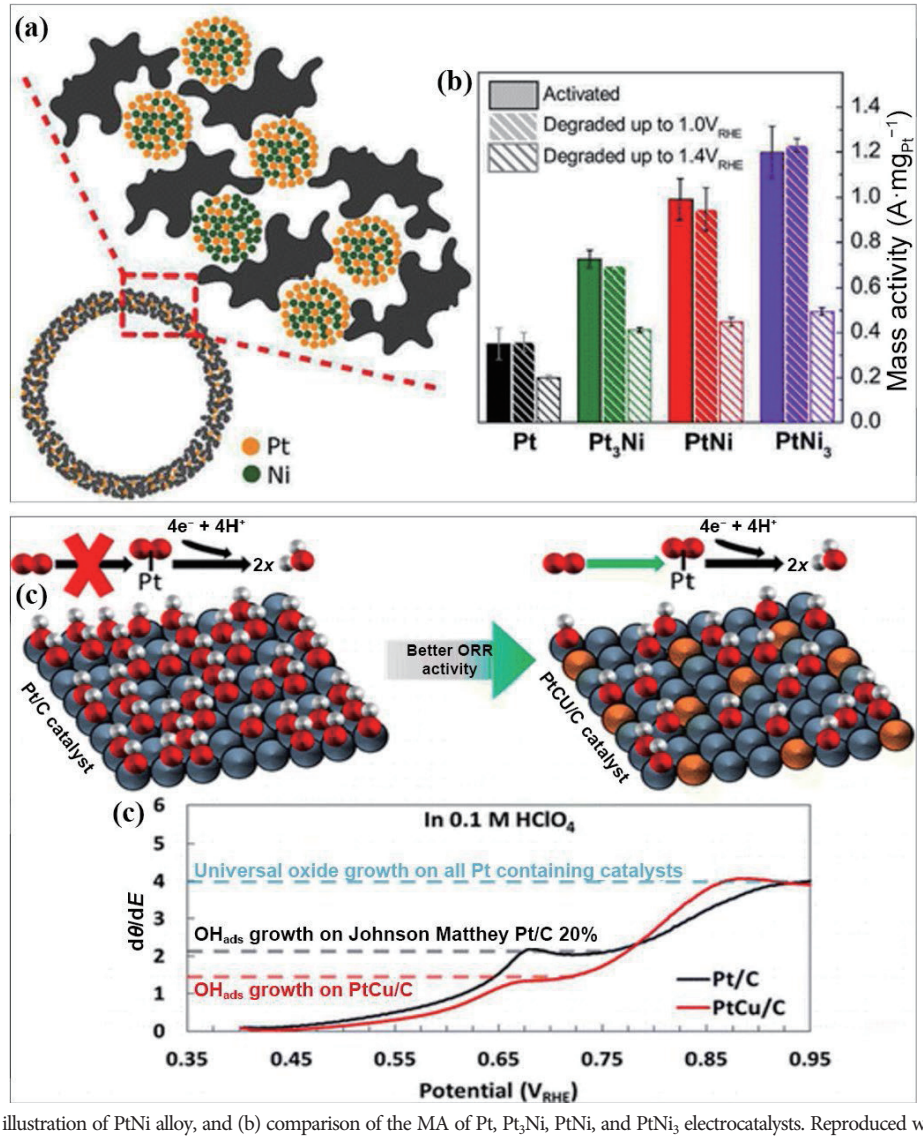

Figure 7 (a) Schematic illustration of PtNi alloy, and (b) comparison of the MA of Pt, Pt_3Ni, PtNi, and $PtNi_3$ electrocatalysts. Reproduced with permission from Ref. [90], © American Chemical Society 2016. (c) Schematic illustration of PtCu alloy, and (d) rate of change of reversible OH_{ads} coverage versus the potential for as-prepared PtCu/C and commercial Pt/C catalysts in 0.1 M $HClO_4$ medium. Reproduced with permission from Ref. [91], © American Chemical Society 2015.

with rare-earth elements, specifically yttrium, have been utilized to increase the ORR activity by over seven times, which reduces the required Pt and total material amount. In the investigations of the overlayer composition and quality of Pt_3Y films sputtered from an alloy [97], Pt_3Y films displayed high ORR activity even though an oxide layer covered the Pt_3Y surface, and the electrocatalyst still exceeded expected activity after acid treatment. Pt dichalcogenides have also been considered for enhancing the ORR performance, with $PtTe_2$ performing better than PtS_2 and $PtSe_2$. $PtTe_2$ exhibited a similar onset potential to commercial Pt/C with an 18 mV potential difference. Brandiele et al. [80] reported the utilization of a solid-state technique involving chemical reduction produced engineered PtxY NPs, with the optimal PtxY600h5 catalyst achieving SA of 1.570 mA·cm^{-2} and MA of 0.586 A·mgpt^{-1}.

5.2 Trimetallic alloy

Alloying Pt with transition metals such as copper (Cu), cobalt (Co), and nickel (Ni) is a successful engineering to reduce the Pt content and enhance the electrocatalytic activity. Rational compositing of Pt with multiple metals has been studied and proven to lead to optimized activities. Several studies have reported a significant improvement in ORR activity by using binary Pt alloys, such as Pt_xCu_y, in either alkaline or acidic media, but concerns arise related to their stability. To investigate the stability issue, Tu et al. [98] synthesized a $Pt_2CuW_{0.25}$ trimetallic alloy by incorporating tungsten (W) atoms into PtCu alloys using wet chemistry. The obtained alloy showed both improved activity and stability for ORR. After 30k cycles, the $Pt_2CuW_{0.25}$/C catalyst maintained its high-efficiency activity, indicating that incorporating W atoms helps stabilize the alloy. The remarkable activity can be ascribed to the stronger interface relation between W and Pt/Cu, which acts as an "adhesive" and makes the Cu atoms less likely to dissolve.

Trimetallic catalysts have exhibited promising developments that can be attributed to the synergistic effect between metal atoms. Interestingly, the metal presence can oxidize the adsorbed intermediate species on the surface of Pt atoms at quite low potential and enhance the active Pt site regeneration. For instance, Dai and co-workers [99] discovered that a Co@Pd-Pt nanocatalyst exhibits enhanced MA with a factor of 30.6 compared to Pt/C catalyst. Similarly, Liu's [100] group synthesized ternary PtAuNi/C via fast microwave-assisted polyol reduction. The prepared PtAuNi/C demonstrated longer-term stability and higher activity in single cell and half cell accelerated degradation tests compared with Pt/C. The incorporation of Au metal into binary Pt-Ni composite enhanced stability as well as improved activity. Recently, researchers developed and utilized several trimetallic Pt-based electrocatalysts for ORR, as summarized in Table 4.

Table 4 Comparative overview of the ORR of trimetallic Pt electrocatalysts in 0.1 M $HClO_4$

Electrocatalyst	SA ($mA·cm^{-2}$)	MA ($A·mgpt^{-1}$)	ECSA ($m^2·g^{-1}$)	Accelerated durability test (cycles)
Pd@PtNi NSs-2 [14]	1.251	1.038	249.88	10,000
Nanoporous Au–Pd–Pt [101]	0.942	1.632	—	70,000
PtPdCu trimetallic octahedrons [102]	0.82	0.51	62	10,000
Trimetallic PtCoFe alloy [103]	4.18	2.59	—	10,000
$Pt_{25}Ir_{20}Co_{55}$ [104]	0.63	0.72	116	20,000
Ag@PtCo-rGO [105]	0.63	0.45	132.06	40,000
Pt_2NiCo/C [106]	1.78	0.53	29.88	5000
PtPdNi octahedral nanocages [107]	1.52	1.14	55.7	10,000
PtNiCo-16h/C nanoflower catalyst [108]	2.47	0.542	22	10,000
$(Ni_{80}Pd_{20})Pt_{20}/C$ [109]	0.047	0.084	175.12	—
NiPdPt/C [110]	0.25	0.202	80.78	1000
PtPdRu dendritic nanocages [111]	2.9@0.6 V	2.61@0.6 V	96.8	10,000
AgPdPt mesoporous nanotubes [112]	1.11@0.85 V	0.61@0.85	54.7	5000
PtNiRh/C trimetallic NWs/C [113]	2.71@0.85 V	2.88@0.85 V	106.4	10,000

5.3 Intermetallic

Intermetallic alloys involve the formation of distinct chemical compounds with precise ratio of metallic elements. Various factors, such as the arrangement of atoms, significantly impact the crystal structure and surface characteristics of intermetallic compounds, leading to variations in both the strength of chemical species adsorption and the nature of chemical reactions, ultimately resulting in different catalytic properties [114]. The well-ordered atomic arrangement of inter-metallic compounds offers increased strain and ligand effects, which can account for their superior catalytic activity when compared with random alloys [115]. Furthermore, intermetallic compounds exhibit enhanced selectivity due to the isolated active sites, which allows for the site-isolation effect and remarkable stability due to the abundant heteroatomic bonding [115].

However, preparing intermetallic catalysts necessitates a high-temperature process to facilitate atomic diffusion and order, which can lead to metal sintering and larger grain size, posing a challenge in practical production. Despite this, Liang and co-workers [116] successfully designed a series of Pt intermetallic compounds on porous sulfur-doped carbon carriers, accomplishing an average NPs size of < 5 nm using a high-temperature sulfur-anchored synthesis method (Fig. 8(a)). The series comprised ternary, quaternary, quinary, and senary Pt intermetallic compounds, each exhibiting a tetragonal ordered P4/mmm space group structure. These intermetallic compound catalysts displayed exceptional activity ranging from 1.3–1.8 $A·mgpt^{-1}$ at 0.9 V vs. RHE, with the Pt-Ni intermetallic exhibiting the highest ORR MA of 1.84 $A·mgpt^{-1}$ at 0.9 V vs. RHE and the Pt–Co intermetallic achieving a high-power density of 1.08 $W·cm^{-2}$ with an ultra-low Pt loading (0.02 $mgPt·cm^{-2}$) hydrogen fuel cell test.

Sun et al. [117] developed a new type of strong hard magnetic $L1_0$-CoPt nanoalloy catalyst possessing a tetragonal crystal structure (Fig. 8(b)). This structure orders the Pt and Co metals in staggered layers, allowing for an optimal Pt–Pt bond distance on the composite surface. As a result, the interaction of the Pt surface with oxygen-containing substances in the ORR is optimized, and the corrosion problem of Co metal under the fuel cell operating environment of 60 to 80 °C is solved. This specific crystal structure substantially increases its oxygen reduction catalytic performance and stability. In the fuel cell tests, $L1_0$-CoPt/Pt initially attains MA of 0.56 $A·mgpt^{-1}$, which decreases to 0.45 $A·mgpt^{-1}$ after potential 30,000 cycles in the membrane electrode assembly at 80 °C.

Several research groups have reported on synthesizing advanced electrocatalysts with improved ORR activity and stability. Joo and co-worker s[115] prepared PtCu nanoframes (O-PtCu NF/C) with an atomically ordered intermetallic structure using a silica-coating-mediated method, resulting in an electrocatalyst with increased active surface area, comfort reactant accessibility, and enhanced strain and ligand effects (Fig. 8(c)). This electrocatalyst exhibited excellent ORR activity and stability. Meanwhile, Shao and co-workers [118] extended a PtFe-N-C electrocatalyst with an ultralow Pt loading that consisted of PtFe alloy on very well dispersed single Pt and Fe atoms in N-doped carbon (Fig. 8(d)). The Pt-$N1C_3$, Fe-$N1C_3$, and PtFe@Pt multiple active sites synergistically enabled the electrocatalyst to exhibit 3.7 times higher Pt MA than Pt/C and excellent durability. Liu et al. [119] developed an electrocatalyst containing ultralow-loading strained Pt-Co core–shell NPs through zeolitic imidazolate frameworks as precursors, which enhanced ORR performance (Fig. 8(e)). Finally, Abruña et al. [120] reported Pt-Co nanocatalysts containing an ordered Pt_3Co intermetallic core and a thin Pt shell, which exhibited over 200% increase in ORR MA compared to disordered Pt_3Co alloy NPs (Fig. 8(f)). These studies demonstrated promising materials for electrocatalytic ORR applications.

6 Single-atom electrocatalysts (SAEs) strategy

The efficient utilization of noble metals in electrocatalysts is crucial for sustainable energy conversion technologies. To apply PEMFCs on a large scale use in vehicles, highly active electrocatalysts with low Pt utilization are essential for cathodes during ORR. SAEs are regarded a promising approach to reduce noble metal usage for decreasing the overall cost to improve economy [121]. Recently, researchers are focusing to design SAEs due to their maximum efficiency of atom utilization, excellent selectivity, high MA, and unique structure [122]. The SAEs strategy has emerged as an effective method to enhance Pt utilization efficiency due to the high concentration of low-coordinated surface Pt atoms in small Pt NPs [123]. These low-coordinated surface atoms can directly participate in the ORR mechanism. Furthermore, atomically dispersed Pt SAEs can achieve 100% Pt utilization efficiency, which makes them an attractive alternative to traditional Pt-based electrocatalysts. Over the last decade, there has been a rising

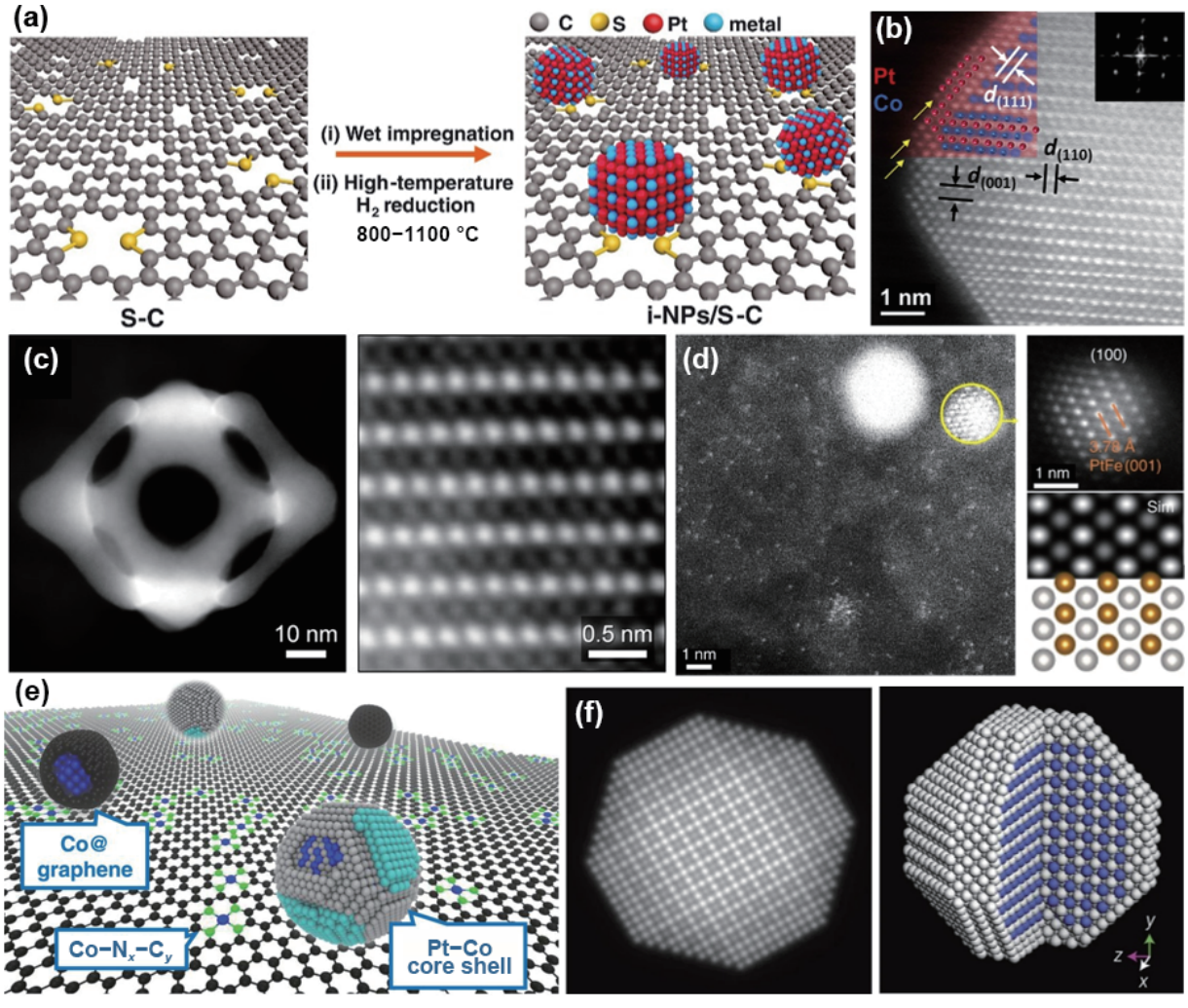

Figure 8 (a) Schematic of the high-temperature S-anchoring synthetic strategy for Pt-based intermetallic. Reproduced with permission from Ref. [116], © Yang, C. L. et al. 2021, some rights reserved; exclusive licensee American Association for the Advancement of Science. (b) STEM image shows 2–3 layers of Pt shell in L10-CoPt/Pt NPs. Reproduced with permission from Ref. [117], © Elsevier Inc. 2018. (c) HAADF-STEM images of O-PtCu NF/C. Reproduced with permission from Ref. [115], © American Chemical Society 2020. (d) HAADF-STEM images ofPtFe-N-C catalyst. Reproduced with permission from Ref. [118], © Xiao, F. et al. 2022. (e) Schematics revealing the coexistence of PtCo NPs, Co/graphene, and CoNxCy active sites. Reproduced with permission from Ref. [119], © Chong, L. et al., some rights reserved; exclusive licensee American Association for the Advancement of Science. (f) Simulated HAADF-STEM image of the Pt_3Co core-shell intermetallic NPs. Reproduced with permission from Ref. [120], © Springer Nature Limited 2012.

interest in developing SAEs due to the strong interaction between Pt metals and supporting materials. As a result, many ORR SAEs have been reported [124].

Some researchers doubt that a single Pt atom can dissociate the oxygen–oxygen bond via lateral adsorption, making the oxygen reduction process yield a 2-electron product, H_2O_2, instead of the 4-electron product required for fuel cells. Nevertheless, Yang et al. [125] conducted experiments and showed that a single Pt atom on titanium carbide (Pt1/TiC) has high activity and stability for electrochemical H_2O_2 production. DFT calculations also revealed that Pt1/TiC is better at preserving the oxygen–oxygen bond and has a higher selectivity towards H_2O_2 production. Likewise, Liu and co-workers [30] studied a single Pt atom electrocatalyst supported on efficient, economical, and stable carbon black, demonstrating carbon monoxide/methanol tolerance. The results obtained from simulations showed that the most active sites on the single Pt atom were single pyridinic nitrogen anchored single Pt atom centers, regarded for the tolerance of carbon monoxide/methanol and very active for ORR.

Based on recent research by Amal et al. [126], the performance of single Pt atom sites as an electrocatalyst can be enhanced through careful coordination structure design. This design innovation improves the selectivity of the reaction and enables 4-electron oxygen reduction in Pt single-atoms. Here, Amal et al. chose phosphorus, which has more valence electrons, to participate in constructing the Pt atomic active sites. The researchers constructed and predicted various coordination configurations of Pt atoms through the DFT theoretical simulations. They found that when phosphorus atoms replaced the α-carbon in the Pt-N_3 site, the center of the d-band of Pt became deeper, thereby favoring oxygen restoration. Additionally, the researchers successfully synthesized this catalyst, which only contained 0.026 wt.% Pt but exhibited oxygen reduction activity comparable to commercial Pt/C (20 wt.%), corresponding to an activity of about 170 times that of Pt/C.

7 Conclusion and perspectives

This critical review shows an overview of recent strategies in developing low-cost, rational engineering, and high-activity Pt-based electrocatalysts for the ORR. In the past decade, novel strategies have been employed to engineer more active Pt electrocatalysts. Synthesis techniques, including those involving morphology, supporting materials, bimetallic and trimetallic alloys, and single-atom Pt electrocatalysts, play crucial roles in determining the electrocatalyst activity and durability. Several

strategies have been used to boost their activity and stability. First, controllable syntheses of Pt-based electrocatalysts with optimized atomic arrangements and surface reactivity have been developed to improve their morphology. The electrocatalyst architecture and morphology are designed to maximize active sites. Second, increasing the contact area between Pt NPs and supporting materials can prevent particle detachment, migration, and accumulation and improve oxidation resistance. Third, alloying Pt with transition metals can reduce the ORR kinetics obstacles observed in pristine Pt electrocatalysts. Including the appropriate noble or transition metals can improve Pt atom dispersion and specific activity. Fourth, the stability of Pt alloy electrocatalysts has been found to rely primarily on the degree of alloying. The introduction of synergetic components can controllably modulate geometrical and electronic structures to control selectivity, activity, and stability, presenting opportunities for the advancement of state-of-the-art ORR electrocatalysts. Finally, engineering Pt SAEs with atomic efficiencies, atomic dispersion, tunable electronic properties, and geometric morphologies can contribute to a deeper understanding of basic electrocatalytic processes and provide a next-generation electrocatalyst for renewable electrochemical energy conversion technologies.

Addressing fundamental issues is crucial for developing Pt-based electrocatalysts for ORR. Several key issues and perspectives deserve further attention: Firstly, exploring advanced synthetic strategies for Pt-based electrocatalysts, such as structural engineering or alloying, is expected to remain a hot topic for researchers. These strategies can provide a broader range of applications and greatly enhance the electrocatalyst properties. Secondly, optimizing electrocatalytic active centers by tuning the electrocatalyst composition, size, and shape is essential for achieving excellent design. Pt alloy composition has been confirmed to take part a critical role in balancing electrocatalytic activity and stability. Using multi-metallic and high-entropy Pt-based alloys allows for increased functionality in ORR. Thirdly, developing novel and low-cost strategies to produce supported Pt-based electrocatalysts with well-defined morphology remains a key interest area. Materials supporting well-defined Pt- based NPs structures are the most effective in PEMFC applications. Control of experimental parameters is required to synthesize optimally sized and monodispersed Pt-alloy nanocomposites. Fourth, developing the electrocatalysts with high activity, excellent selectivity, and outstanding stability is always the key task and ultimate goal in large scale industrial production. Therefore, researchers should focus on designing economical strategies to overcome the gap between laboratory and large-scale industrial production.

Finally, despite the remarkable achievements, improved Pt-based SAEs are still needed for commercial application. Major challenges such as large resistance, sluggish mass transport, and poor durability must be addressed. Additionally, the mechanism description and structure identification require more research. These challenges present exciting opportunities for the development of Pt-based SAEs, which can inspire more advanced research for renewable energy conversion and storage technologies.

Acknowledgements

A. A., G. H., S. H., A. L., and X. Y. J. thank the financial support from Kempe Foundation (SMK21-0011, SMK21-0020). A. L. acknowledges Swedish Research Council (2019-03865) and European Union's Horizon Europe research and innovation program under grant agreement No. 101086667. X. Y. J. thanks the financial support from Horizon-EIC and Pathfinder challenges, Grant Number: 101070976.

Funding note: Open access funding provided by Lulea University of Technology.

References

[1] Wang, Y. J.; Zhao, N. N.; Fang, B. Z.; Li, H.; Bi, X. T.; Wang, H. J. Carbon-supported Pt-based alloy electrocatalysts for the oxygen reduction reaction in polymer electrolyte membrane fuel cells: Particle size, shape, and composition manipulation and their impact to activity. *Chem. Rev.* **2015**, *115*, 3433–3467.

[2] Ali, A.; Shen, P. K. Recent advances in graphene-based platinum and palladium electrocatalysts for the methanol oxidation reaction. *J. Mater. Chem. A* **2019**, *7*, 22189–22217.

[3] Ali, A.; Shen, P. K. Nonprecious metal's graphene-supported electrocatalysts for hydrogen evolution reaction: Fundamentals to applications. *Carbon Energy* **2020**, *2*, 99–121.

[4] Sui, S.; Wang, X. Y.; Zhou, X. T.; Su, Y. H.; Riffat, S.; Liu, C. J. A comprehensive review of Pt electrocatalysts for the oxygen reduction reaction: Nanostructure, activity, mechanism and carbon support in PEM fuel cells. *J. Mater. Chem. A* **2017**, *5*, 1808–1825.

[5] Ali, A.; Shen, P. K. Recent progress in graphene-based nanostructured electrocatalysts for overall water splitting. *Electrochem. Energy Rev.* **2020**, *3*, 370–394.

[6] Singh, K.; Tetteh, E. B.; Lee, H. Y.; Kang, T. H.; Yu, J. S. Tailor-made Pt catalysts with improved oxygen reduction reaction stability/durability. *ACS Catal.* **2019**, *9*, 8622–8645.

[7] Sharma, M.; Jung, N.; Yoo, S. J. Toward high-performance Pt-based nanocatalysts for oxygen reduction reaction through organic-inorganic hybrid concepts. *Chem. Mater.* **2018**, *30*, 2–24.

[8] Kulkarni, A.; Siahrostami, S.; Patel, A.; Nørskov, J. K. Understanding catalytic activity trends in the oxygen reduction reaction. *Chem. Rev.* **2018**, *118*, 2302–2312.

[9] Nie, Y.; Li, L.; Wei, Z. D. Recent advancements in Pt and Pt-free catalysts for oxygen reduction reaction. *Chem. Soc. Rev.* **2015**, *44*, 2168–2201.

[10] Zhou, Y.; Chen, B. Investigation of optimization and evaluation criteria for flow field in proton exchange membrane fuel cell: A critical review. *Renew. Sustain. Energy Rev.* **2023**, *185*, 113584.

[11] Van Der Linden, F.; Pahon, E.; Morando, S.; Bouquain, D. A review on the proton-exchange membrane fuel cell break-in physical principles, activation procedures, and characterization methods. *J. Power Sources* **2023**, *575*, 233168.

[12] Hao, C.; Meng, Q. H.; Yan, B. W.; Liu, J.; Yang, B.; Feng, L. G.; Shen, P. K.; Tian, Z. Q. Efficient catalyst layer with ultra-low Pt loading for proton exchange membrane fuel cell. *Chem. Eng. J.* **2023**, *472*, 144945.

[13] Shao, M. H.; Chang, Q. W.; Dodelet, J. P.; Chenitz, R. Recent advances in electrocatalysts for oxygen reduction reaction. *Chem. Rev.* **2016**, *116*, 3594–3657.

[14] Chen, Q. Y.; Chen, Z. Y.; Ali, A.; Luo, Y. Q.; Feng, H. Y.; Luo, Y.

Y.; Tsiakaras, P.; Shen, P. K. Shell-thickness-dependent Pd@PtNi core–shell nanosheets for efficient oxygen reduction reaction. *Chem. Eng. J.* **2022**, *427*, 131565.

[15] Gómez-Marín, A. M.; Ticianelli, E. A. A reviewed vision of the oxygen reduction reaction mechanism on Pt-based catalysts. *Curr. Opin. Electrochem.* **2018**, *9*, 129–136.

[16] Lyu, D. D.; Yao, S. X.; Ali, A.; Tian, Z. Q.; Tsiakaras, P.; Shen, P. K. N, S codoped carbon matrix-encapsulated Co_9S_8 nanoparticles as a highly efficient and durable bifunctional oxygen redox electrocatalyst for rechargeable Zn-air batteries. *Adv. Energy Mater.* **2021**, *11*, 2101249.

[17] Gan, T.; Wang, D. S. Atomically dispersed materials: Ideal catalysts in atomic era. *Nano Res.*, in press, https://doi.org/10.1007/s12274-023-5700-4.

[18] Sakthivel, M.; Drillet, J. F. An extensive study about influence of the carbon support morphology on Pt activity and stability for oxygen reduction reaction. *Appl. Catal. B Environ.* **2018**, *231*, 62–72.

[19] Banham, D.; Ye, S. Y.; Pei, K.; Ozaki, J. I.; Kishimoto, T.; Imashiro, Y. A review of the stability and durability of non-precious metal catalysts for the oxygen reduction reaction in proton exchange membrane fuel cells. *J. Power Sources* **2015**, *285*, 334–348.

[20] Hu, S. Q.; Li, X. L.; Ali, A.; Zhang, X. Y.; Shen, P. K. Large-scale synthesis of porous Pt nanospheres/three-dimensional graphene hybrid materials as a highly active and stable electrocatalyst for oxygen reduction reaction. *ChemistrySelect* **2021**, *6*, 2080–2084.

[21] Stacy, J.; Regmi, Y. N.; Leonard, B.; Fan, M. H. The recent progress and future of oxygen reduction reaction catalysis: A review. *Renew. Sustain. Energy Rev.* **2017**, *69*, 401–414.

[22] Huang, L.; Zhang, X. P.; Wang, Q. Q.; Han, Y. J.; Fang, Y. X.; Dong, S. J. Shape-control of Pt-Ru nanocrystals: Tuning surface structure for enhanced electrocatalytic methanol oxidation. *J. Am. Chem. Soc.* **2018**, *140*, 1142–1147.

[23] Shi, Y. F.; Lyu, Z. H.; Zhao, M.; Chen, R. H.; Nguyen, Q. N.; Xia, Y. N. Noble-metal nanocrystals with controlled shapes for catalytic and electrocatalytic applications. *Chem. Rev.* **2021**, *121*, 649–735.

[24] Kim, C.; Dionigi, F.; Beermann, V.; Wang, X. L.; Möller, T.; Strasser, P. Alloy nanocatalysts for the electrochemical oxygen reduction (ORR) and the direct electrochemical carbon dioxide reduction reaction (CO_2RR). *Adv. Mater.* **2019**, *31*, 1805617.

[25] Luo, Y.; Alonso-Vante, N. The effect of support on advanced Pt-based cathodes towards the oxygen reduction reaction. *State of the Art. Electrochim. Acta* **2015**, *179*, 108–118.

[26] Li, C. L.; Tan, H. B.; Lin, J. J.; Luo, X. L.; Wang, S. P.; You, J.; Kang, Y. M.; Bando, Y.; Yamauchi, Y.; Kim, J. Emerging Pt-based electrocatalysts with highly open nanoarchitectures for boosting oxygen reduction reaction. *Nano Today* **2018**, *21*, 91–105.

[27] Wu, D. Z.; Shen, X. C.; Pan, Y. B.; Yao, L. B.; Peng, Z. M. Platinum alloy catalysts for oxygen reduction reaction: Advances, challenges and perspectives. *ChemNanoMat* **2020**, *6*, 32–41.

[28] Zhao, J. Y.; Lian, J.; Zhao, Z. X.; Wang, X. M.; Zhang, J. J. A review of *in-situ* techniques for probing active sites and mechanisms of electrocatalytic oxygen reduction reactions. *Nano-Micro Lett.* **2023**, *15*, 19.

[29] Nayak, S.; McPherson, I. J.; Vincent, K. A. Adsorbed intermediates in oxygen reduction on platinum nanoparticles observed by *in situ* IR spectroscopy. *Angew. Chem.* **2018**, *130*, 13037–13040.

[30] Liu, J.; Jiao, M. G.; Lu, L. L.; Barkholtz, H. M.; Li, Y. P.; Wang, Y.; Jiang, L. H.; Wu, Z. J.; Liu, D. J.; Zhuang, L. et al. High performance platinum single atom electrocatalyst for oxygen reduction reaction. *Nat. Commun.* **2017**, *8*, 15938.

[31] Dong, J. C.; Zhang, X. G.; Briega-Martos, V.; Jin, X.; Yang, J.; Chen, S.; Yang, Z. L.; Wu, D. Y.; Feliu, J. M.; Williams, C. T. et al. *In situ* Raman spectroscopic evidence for oxygen reduction reaction intermediates at platinum single-crystal surfaces. *Nat. Energy* **2019**, *4*, 60–67.

[32] Lu, S. L.; Eid, K.; Deng, Y. Y.; Guo, J.; Wang, L.; Wang, H. J.; Gu, H. W. One-pot synthesis of PtIr tripods with a dendritic surface as an efficient catalyst for the oxygen reduction reaction. *J. Mater. Chem. A* **2017**, *5*, 9107–9112.

[33] Park, J.; Wang, H. L.; Vara, M.; Xia, Y. N. Platinum cubic nanoframes with enhanced catalytic activity and durability toward oxygen reduction. *ChemSusChem* **2016**, *9*, 2855–2861.

[34] Kwon, H.; Kabiraz, M. K.; Park, J.; Oh, A.; Baik, H.; Choi, S. I.; Lee, K. Dendrite-embedded platinum-nickel multiframes as highly active and durable electrocatalyst toward the oxygen reduction reaction. *Nano Lett.* **2018**, *18*, 2930–2936.

[35] Strickler, A. L.; Jackson, A.; Jaramillo, T. F. Active and stable Ir@Pt core–shell catalysts for electrochemical oxygen reduction. *ACS Energy Lett.* **2017**, *2*, 244–249.

[36] Bu, L. Z.; Zhang, N.; Guo, S. J.; Zhang, X.; Li, J.; Yao, J. L.; Wu, T.; Lu, G.; Ma, J. Y.; Su, D. et al. Biaxially strained PtPb/Pt core/shell nanoplate boosts oxygen reduction catalysis. *Science* **2016**, *354*, 1410–1414.

[37] Huang, X. Q.; Zhao, Z. P.; Cao, L.; Chen, Y.; Zhu, E. B.; Lin, Z. Y.; Li, M. F.; Yan, A. M.; Zettl, A.; Wang, Y. M. et al. High-performance transition metal-doped Pt_3Ni octahedra for oxygen reduction reaction. *Science* **2015**, *348*, 1230–1234.

[38] Park, J.; Zhang, L.; Choi, S. I.; Roling, L. T.; Lu, N.; Herron, J. A.; Xie, S. F.; Wang, J. G.; Kim, M. J.; Mavrikakis, M. et al. Atomic layer-by-layer deposition of platinum on palladium octahedra for enhanced catalysts toward the oxygen reduction reaction. *ACS Nano* **2015**, *9*, 2635–2647.

[39] Tian, X. L.; Zhao, X.; Su, Y. Q.; Wang, L. J.; Wang, H. M.; Dang, D.; Chi, B.; Liu, H. F.; Hensen, E. J. M.; Lou, X. W. et al. Engineering bunched Pt-Ni alloy nanocages for efficient oxygen reduction in practical fuel cells. *Science* **2019**, *366*, 850–856.

[40] Li, M. F.; Zhao, Z. P.; Cheng, T.; Fortunelli, A.; Chen, C. Y.; Yu, R.; Zhang, Q. H.; Gu, L.; Merinov, B. V.; Lin, Z. Y. et al. Ultrafine jagged platinum nanowires enable ultrahigh mass activity for the oxygen reduction reaction. *Science* **2016**, *354*, 1414–1419.

[41] Wu, R. F.; Tsiakaras, P.; Shen, P. K. Facile synthesis of bimetallic Pt-Pd symmetry-broken concave nanocubes and their enhanced activity toward oxygen reduction reaction. *Appl. Catal. B Environ.* **2019**, *251*, 49–56.

[42] Zhu, X. X.; Huang, L.; Wei, M.; Tsiakaras, P.; Shen, P. K. Highly stable Pt-Co nanodendrite in nanoframe with Pt skin structured catalyst for oxygen reduction electrocatalysis. *Appl. Catal. B Environ.* **2021**, *281*, 119460.

[43] Hu, S. Q.; Wang, Z.; Chen, H. L.; Wang, S. B.; Li, X. G.; Zhang, X. Y.; Shen, P. K. Ultrathin PtCo nanorod assemblies with self-optimized surface for oxygen reduction reaction. *J. Electroanal. Chem.* **2020**, *870*, 114194.

[44] Wu, R. F.; Li, Y. J.; Gong, W. H.; Shen, P. K. One-pot synthesis of Pt-Pd bimetallic nanodendrites with enhanced electrocatalytic activity for oxygen reduction reaction. *ACS Sustain. Chem. Eng.* **2019**, *7*, 8419–8428.

[45] Chen, H. L.; Wu, R. F.; Shen, P. K. One-pot fabrication of site-selective hexapod PtPdCu concave rhombic dodecahedrons as highly efficient catalysts for electrocatalysis. *ACS Sustain. Chem. Eng.* **2020**, *8*, 1520–1526.

[46] Ma, L.; Wang, C. M.; Xia, B. Y.; Mao, K. K.; He, J. W.; Wu, X. J.; Xiong, Y. J.; Lou, X. W. Platinum multicubes prepared by Ni^{2+}-mediated shape evolution exhibit high electrocatalytic activity for oxygen reduction. *Angew. Chem., Int. Ed.* **2015**, *54*, 5666–5671.

[47] Zhang, W. C.; Li, F.; Shi, F. L.; Hu, H.; Liang, J.; Yang, H. Y.; Ye, Y. L.; Mao, Z. S.; Shang, W.; Deng, T. et al. Tensile-strained platinum-cobalt alloy surface on palladium octahedra as a highly durable oxygen reduction catalyst. *ACS Appl. Mater. Interfaces* **2023**, *15*, 3993–4000.

[48] Chen, G. Y.; Kuttiyiel, K. A.; Li, M.; Su, D.; Du, L.; Du, C. Y.; Gao, Y. Z.; Fei, W. D.; Yin, G. P.; Sasaki, K. et al. Correlating the electrocatalytic stability of platinum monolayer catalysts with their structural evolution in the oxygen reduction reaction. *J. Mater. Chem. A* **2018**, *6*, 20725–20736.

[49] Zhang, L. L.; Zhu, S. Q.; Chang, Q. W.; Su, D.; Yue, J.; Du, Z.; Shao, M. H. Palladium-platinum core-shell electrocatalysts for oxygen reduction reaction prepared with the assistance of citric acid. *ACS Catal.* **2016**, *6*, 3428–3432.

[50] Wang, Z. X.; Yao, X. Z.; Kang, Y. Q.; Miao, L. Q.; Xia, D. S.; Gan, L. Structurally ordered low-Pt intermetallic electrocatalysts

toward durably high oxygen reduction reaction activity. *Adv. Funct. Mater.* **2019**, *29*, 1902987.

[51] Li, J. R.; Xi, Z.; Pan, Y. T.; Spendelow, J. S.; Duchesne, P. N.; Su, D.; Li, Q.; Yu, C.; Yin, Z. Y.; Shen, B. et al. Fe stabilization by intermetallic $L1_0$-FePt and Pt catalysis enhancement in $L1_0$-FePt/Pt nanoparticles for efficient oxygen reduction reaction in fuel cells. *J. Am. Chem. Soc.* **2018**, *140*, 2926–2932.

[52] Hoque, A.; Hassan, F. M.; Higgins, D.; Choi, J. Y.; Pritzker, M.; Knights, S.; Ye, S. Y.; Chen, Z. W. Multigrain platinum nanowires consisting of oriented nanoparticles anchored on sulfur-doped graphene as a highly active and durable oxygen reduction electrocatalyst. *Adv. Mat.* **2015**, *27*, 1229–1234.

[53] Chen, Y. L.; Cheng, T.; Goddard III, W. A. Atomistic explanation of the dramatically improved oxygen reduction reaction of jagged platinum nanowires, 50 times better than Pt. *J. Am. Chem. Soc.* **2020**, *142*, 8625–8632.

[54] Ma, Y. L.; Gao, W. P.; Shan, H.; Chen, W. L.; Shang, W.; Tao, P.; Song, C. Y.; Addiego, C.; Deng, T.; Pan, X. Q. et al. Platinum-based nanowires as active catalysts toward oxygen reduction reaction: *In situ* observation of surface-diffusion-assisted, solid-state oriented attachment. *Adv. Mater.* **2017**, *29*, 1703460.

[55] Jin, H.; Xu, Z. W.; Hu, Z. Y.; Yin, Z.; Wang, Z.; Deng, Z.; Wei, P.; Feng, S. L.; Dong, S. H.; Liu, J. F. et al. Mesoporous Pt@Pt-skin Pt_3Ni core–shell framework nanowire electrocatalyst for efficient oxygen reduction. *Nat. Commun.* **2023**, *14*, 1518.

[56] Zhu, J. L.; He, G. Q.; Tian, Z. Q.; Liang, L. Z.; Shen, P. K. Facile synthesis of boron and nitrogen-dual-doped graphene sheets anchored platinum nanoparticles for oxygen reduction reaction. *Electrochim. Acta* **2016**, *194*, 276–282.

[57] Kim, T. H.; Jung, C. Y.; Bose, R.; Yi, S. C. Cobalt encapsulated in the nitrogen and sulfur co-doped carbon nanotube supported platinum for the oxygen reduction reaction catalyst. *Carbon* **2018**, *139*, 656–665.

[58] Yu, F. Y.; Xie, Y. J.; Wang, L. K.; Yang, N. T.; Meng, X. X.; Wang, X. B.; Tian, X. L.; Yang, X. Platinum supported on multifunctional titanium cobalt oxide nanosheets assembles for efficient oxygen reduction reaction. *Electrochim. Acta* **2018**, *265*, 364–371.

[59] Teran-Salgado, E.; Bahena-Uribe, D.; Márquez-Aguilar, P. A.; Reyes-Rodriguez, J. L.; Cruz-Silva, R.; Solorza-Feria, O. Platinum nanoparticles supported on electrochemically oxidized and exfoliated graphite for the oxygen reduction reaction. *Electrochim. Acta* **2019**, *298*, 172–185.

[60] Hussain, S.; Kongi, N.; Erikson, H.; Rähn, M.; Merisalu, M.; Matisen, L.; Paiste, P.; Aruväli, J.; Sammelselg, V.; Estudillo-Wong, L. A. et al. Platinum nanoparticles photo-deposited on SnO_2-C composites: An active and durable electrocatalyst for the oxygen reduction reaction. *Electrochim. Acta* **2019**, *316*, 162–172.

[61] Nan, H. X.; Dang, D.; Tian, X. L. Structural engineering of robust titanium nitride as effective platinum support for the oxygen reduction reaction. *J. Mater. Chem. A* **2018**, *6*, 6065–6073.

[62] Hoque, A.; Hassan, F. M.; Seo, M. H.; Choi, J. Y.; Pritzker, M.; Knights, S.; Ye, S. Y.; Chen, Z. W. Optimization of sulfur-doped graphene as an emerging platinum nanowires support for oxygen reduction reaction. *Nano Energy* **2016**, *19*, 27–38.

[63] Cheng, N. C.; Banis, M. N.; Liu, J.; Riese, A.; Li, X.; Li, R. Y.; Ye, S. Y.; Knights, S.; Sun, X. L. Extremely stable platinum nanoparticles encapsulated in a zirconia nanocage by area-selective atomic layer deposition for the oxygen reduction reaction. *Adv. Mater.* **2015**, *27*, 277–281.

[64] Zheng, Y. Y.; Zhang, J.; Zhan, H. T.; Sun, D. L.; Dang, D.; Tian, X. L. Porous and three dimensional titanium nitride supported platinum as an electrocatalyst for oxygen reduction reaction. *Electrochem. Commun.* **2018**, *91*, 31–35.

[65] Hu, S. Q.; Liu, Y. Y.; Wang, S. B.; Zhang, X. Y.; Shen, P. K. Ultrathin Co_3O_4-Pt core–shell nanoparticles coupled with three-dimensional graphene for oxygen reduction reaction. *Int. J. Hyd. Energy* **2021**, *46*, 10303–10311.

[66] Xu, C. X.; Fan, C. C.; Zhang, X. L.; Chen, H. T.; Liu, X. T.; Fu, Z. M.; Wang, R. R.; Hong, T.; Cheng, J. G. MXene ($Ti_3C_2T_x$) and carbon nanotube hybrid-supported platinum catalysts for the high-performance oxygen reduction reaction in PEMFC. *ACS Appl. Mater. Interfaces* **2020**, *12*, 19539–19546.

[67] Mirshekari, G. R.; Rice, C. A. Effects of support particle size and Pt content on catalytic activity and durability of Pt/TiO_2 catalyst for oxygen reduction reaction in proton exchange membrane fuel cells environment. *J. Power Sources* **2018**, *396*, 606–614.

[68] Mo, R. C.; Zhang, X. R.; Chen, Z. Y.; Huang, S. L.; Li, Y. J.; Liang, L. Z.; Tian, Z. Q.; Shen, P. K. Highly efficient PtCo nanoparticles on Co-N-C nanorods with hierarchical pore structure for oxygen reduction reaction. *Int. J. Hyd. Energy* **2021**, *46*, 15991–16002.

[69] Gao, Y. F.; Uchiyama, T.; Yamamoto, K.; Watanabe, T.; Thakur, N.; Sato, R.; Teranishi, T.; Imai, H.; Sakurai, Y.; Uchimoto, Y. Protection against absorption passivation on platinum by a nitrogen-doped carbon shell for enhanced oxygen reduction reaction. *ACS Appl. Mater. Interfaces* **2023**, *15*, 30240–30248.

[70] Park, J. H.; Kim, K.; Wang, X. Y.; Huda, M.; Sawada, Y.; Matsuo, Y.; Saito, N.; Kawasumi, M. Highly durable graphene-encapsulated platinum-based electrocatalyst for oxygen reduction reactions synthesized by solution plasma process. *J. Power Sources* **2023**, *580*, 233419.

[71] Ma, Z. H.; Tian, H.; Meng, G.; Peng, L. X.; Chen, Y. F.; Chen, C.; Chang, Z. W.; Cui, X. Z.; Wang, L. J.; Jiang, W. et al. Size effects of platinum particles@CNT on HER and ORR performance. *Sci. China Mater.* **2020**, *63*, 2517–2529.

[72] Zhu, J. L.; Wei, P. C.; Li, K. K.; He, S. B.; Pan, Z. Y.; Nie, S. X.; Key, J.; Shen, P. K. Self-assembled nanofiber networks of well-separated B and N codoped carbon as Pt supports for highly efficient and stable oxygen reduction electrocatalysis. *ACS Sustain. Chem. Eng.* **2019**, *7*, 660–668.

[73] Lin, G. X.; Ju, Q. J.; Jin, Y.; Qi, X. H.; Liu, W. J.; Huang, F. Q.; Wang, J. C. Suppressing dissolution of Pt-based electrocatalysts through the electronic metal–support interaction. *Adv. Energy Mater.* **2021**, *11*, 2101050.

[74] Zhao, S.; Wangstrom, A. E.; Liu, Y.; Rigdon, W. A.; Mustain, W. E. Stability and activity of Pt/ITO electrocatalyst for oxygen reduction reaction in alkaline media. *Electrochim. Acta* **2015**, *157*, 175–182.

[75] Hsieh, B. J.; Tsai, M. C.; Pan, C. J.; Su, W. N.; Rick, J.; Lee, J. F.; Yang, Y. W.; Hwang, B. J. Platinum loaded on dual-doped TiO_2 as an active and durable oxygen reduction reaction catalyst. *NPG Asia Mater.* **2017**, *9*, e403.

[76] Estudillo-Wong, L. A.; Luo, Y.; Díaz-Real, J. A.; Alonso-Vante, N. Enhanced oxygen reduction reaction stability on platinum nanoparticles photo-deposited onto oxide-carbon composites. *Appl. Catal. B Environ.* **2016**, *187*, 291–300.

[77] Bu, L. Z.; Guo, S. J.; Zhang, X.; Shen, X.; Su, D.; Lu, G.; Zhu, X.; Yao, J. L.; Guo, J.; Huang, X. Q. Surface engineering of hierarchical platinum-cobalt nanowires for efficient electrocatalysis. *Nat. Commun.* **2016**, *7*, 11850.

[78] Jia, Q. Q.; Liang, W. T.; Bates, M. K.; Mani, P.; Lee, W.; Mukerjee, S. Activity descriptor identification for oxygen reduction on platinum-based bimetallic nanoparticles: *In situ* observation of the linear composition-strain-activity relationship. *ACS Nano* **2015**, *9*, 387–400.

[79] Jung, C.; Lee, C.; Bang, K.; Lim, J.; Lee, H.; Ryu, H. J.; Cho, E.; Lee, H. M. Synthesis of chemically ordered Pt_3Fe/C intermetallic electrocatalysts for oxygen reduction reaction with enhanced activity and durability via a removable carbon coating. *ACS Appl. Mater. Interfaces* **2017**, *9*, 31806–31815.

[80] Brandiele, R.; Durante, C.; Grądzka, E.; Rizzi, G. A.; Zheng, J.; Badocco, D.; Centomo, P.; Pastore, P.; Granozzi, G.; Gennaro, A. One step forward to a scalable synthesis of platinum-yttrium alloy nanoparticles on mesoporous carbon for the oxygen reduction reaction. *J. Mater. Chem. A* **2016**, *4*, 12232–12240.

[81] Chang, F. F.; Yu, G.; Shan, S. Y.; Skeete, Z.; Wu, J. F.; Luo, J.; Ren, Y.; Petkov, V.; Zhong, C. J. Platinum-nickel nanowire catalysts with composition-tunable alloying and faceting for the oxygen reduction reaction. *J. Mater. Chem. A* **2017**, *5*, 12557–12568.

[82] Godínez-Salomón, F.; Mendoza-Cruz, R.; Arellano-Jimenez, M. J.; Jose-Yacaman, M.; Rhodes, C. P. Metallic two-dimensional nanoframes: Unsupported hierarchical nickel-platinum alloy nanoarchitectures with enhanced electrochemical oxygen reduction activity and stability. *ACS Appl. Mater. Interfaces* **2017**, *9*, 18660–18674.

[83] Chang, F. F.; Bai, Z. Y.; Li, M.; Ren, M. Y.; Liu, T. C.; Yang, L.; Zhong, C. J.; Lu, J. Strain-modulated platinum-palladium nanowires for oxygen reduction reaction. *Nano Lett.* **2020**, *20*, 2416–2422.

[84] Yin, S. F.; Xie, Z. Y.; Deng, X. T.; Xuan, W.; Duan, Y. R.; Zhang, S. H.; Liang, Y. L. Simple synthesis of ordered platinum-gold nanoparticles with the enhanced catalytic activity for oxygen reduction reaction. *J. Electroanal. Chem.* **2020**, *856*, 113707.

[85] Zhang, E. H.; Ma, F. F.; Liu, J.; Sun, J. Y.; Chen, W. X.; Rong, H. P.; Zhu, X. Y.; Liu, J. J.; Xu, M.; Zhuang, Z. B. et al. Porous platinum-silver bimetallic alloys: Surface composition and strain tunability toward enhanced electrocatalysis. *Nanoscale* **2018**, *10*, 21703–21711.

[86] Ying, J.; Jiang, G. P.; Cano, Z. P.; Ma, Z.; Chen, Z. W. Spontaneous weaving: 3D porous PtCu networks with ultrathin jagged nanowires for highly efficient oxygen reduction reaction. *Appl. Catal. B Environ.* **2018**, *236*, 359–367.

[87] Čolić, V.; Bandarenka, A. S. Pt alloy electrocatalysts for the oxygen reduction reaction: From model surfaces to nanostructured systems. *ACS Catal.* **2016**, *6*, 5378–5385.

[88] Zhang, L. Z.; Fischer, J. M. T. A.; Jia, Y.; Yan, X. C.; Xu, W.; Wang, X. Y.; Chen, J.; Yang, D. J.; Liu, H. W.; Zhuang, L. Z. et al. Coordination of atomic Co–Pt coupling species at carbon defects as active sites for oxygen reduction reaction. *J. Am. Chem. Soc.* **2018**, *140*, 10757–10763.

[89] Wang, X.; Zhao, Z. L.; Sun, P.; Li, F. W. One-step synthesis of supported high-index faceted platinum-cobalt nanocatalysts for an enhanced oxygen reduction reaction. *ACS Appl. Energy Mater.* **2020**, *3*, 5077–5082.

[90] Mezzavilla, S.; Baldizzone, C.; Swertz, A. C.; Hodnik, N.; Pizzutilo, E.; Polymeros, G.; Keeley, G. P.; Knossalla, J.; Heggen, M.; Mayrhofer, K. J. J. et al. Structure–activity–stability relationships for space-confined Pt_xNi_y nanoparticles in the oxygen reduction reaction. *ACS Catal.* **2016**, *6*, 8058–8068.

[91] Coleman, E. J.; Chowdhury, M. H.; Co, A. C. Insights into the oxygen reduction reaction activity of Pt/C and PtCu/C catalysts. *ACS Catal.* **2015**, *5*, 1245–1253.

[92] Bordley, J. A.; El-Sayed, M. A. Enhanced electrocatalytic activity toward the oxygen reduction reaction through alloy formation: Platinum-silver alloy nanocages. *J. Phys. Chem. C* **2016**, *120*, 14643–14651.

[93] Yavuz, E.; Özdokur, K. V.; Çakar, İ.; Koçak, S.; Ertaş, F. N. Electrochemical preparation, characterization of molybdenum-oxide/platinum binary catalysts and its application to oxygen reduction reaction in weakly acidic medium. *Electrochim. Acta* **2015**, *151*, 72–80.

[94] Wang, X. M.; Orikasa, Y.; Uchimoto, Y. Platinum-based electrocatalysts for the oxygen-reduction reaction: Determining the role of pure electronic charge transfer in electrocatalysis. *ACS Catal.* **2016**, *6*, 4195–4198.

[95] Wang, W.; Wang, Z. Y.; Wang, J. J.; Zhong, C. J.; Liu, C. J. Highly active and stable Pt-Pd alloy catalysts synthesized by room-temperature electron reduction for oxygen reduction reaction. *Adv. Sci.* **2017**, *4*, 1600486.

[96] Huang, H. W.; Li, K.; Chen, Z.; Luo, L. H.; Gu, Y. Q.; Zhang, D. Y.; Ma, C.; Si, R.; Yang, J. L.; Peng, Z. M. et al. Achieving remarkable activity and durability toward oxygen reduction reaction based on ultrathin Rh-doped Pt nanowires. *J. Am. Chem. Soc.* **2017**, *139*, 8152–8159.

[97] Brown, R.; Vorokhta, M.; Khalakhan, I.; Dopita, M.; Vonderach, T.; Skála, T.; Lindahl, N.; Matolínová, I.; Grönbeck, H.; Neyman, K. M. et al. Unraveling the surface chemistry and structure in highly active sputtered Pt_3Y catalyst films for the oxygen reduction reaction. *ACS Appl. Mater. Interfaces* **2020**, *12*, 4454–4462.

[98] Tu, W. Z.; Luo, W. J.; Chen, C. L.; Chen, K.; Zhu, E. B.; Zhao, Z. P.; Wang, Z. L.; Hu, T.; Zai, H. C.; Ke, X. X. et al. Tungsten as "adhesive" in $Pt_2CuW_{0.25}$ ternary alloy for highly durable oxygen reduction electrocatalysis. *Adv. Funct. Mater.* **2020**, *30*, 1908230.

[99] Dai, S.; Chou, J. P.; Wang, K. W.; Hsu, Y. Y.; Hu, A.; Pan, X. Q.; Chen, T. Y. Platinum-trimer decorated cobalt-palladium core–shell nanocatalyst with promising performance for oxygen reduction reaction. *Nat. Commun.* **2019**, *10*, 440.

[100] Liu, F.; Sun, K.; Rui, Z. Y.; Liu, J. G.; Juan, T.; Liu, R. R.; Luo, J.; Wang, Z. W.; Yao, Y. F.; Huang, L. et al. Highly durable and active ternary Pt-Au-Ni electrocatalyst for oxygen reduction reaction. *ChemCatChem* **2018**, *10*, 3049–3056.

[101] Li, J.; Yin, H. M.; Li, X. B.; Okunishi, E.; Shen, Y. L.; He, J.; Tang, Z. K.; Wang, W. X.; Yücelen, E.; Li, C. et al. Surface evolution of a Pt-Pd-Au electrocatalyst for stable oxygen reduction. *Nat. Energy* **2017**, *2*, 17111.

[102] Zhao, R. P.; Chen, Z. J.; Huang, S. M. Rapid synthesis of hollow PtPdCu trimetallic octahedrons at room temperature for oxygen reduction reactions in acid media. *CrystEngComm* **2020**, *22*, 1586–1592.

[103] Sial, M. A. Z. G.; Lin, H. F.; Zulfiqar, M.; Ullah, S.; Ni, B.; Wang, X. Trimetallic PtCoFe alloy monolayer superlattices as bifunctional oxygen-reduction and ethanol-oxidation electrocatalysts. *Small* **2017**, *13*, 1700250.

[104] Loukrakpam, R.; Wanjala, B. N.; Yin, J.; Fang, B.; Luo, J.; Shao, M. H.; Protsailo, L.; Kawamura, T.; Chen, Y. S.; Petkov, V. et al. Structural and electrocatalytic properties of PtIrCo/C catalysts for oxygen reduction reaction. *ACS Catal.* **2011**, *1*, 562–572.

[105] Deng, X. T.; Yin, S. F.; Xie, Z. Y.; Gao, F.; Jiang, S.; Zhou, X. Synthesis of silver@platinum-cobalt nanoflower on reduced graphene oxide as an efficient catalyst for oxygen reduction reaction. *Int. J. Hyd. Energy* **2021**, *46*, 17731–17740.

[106] Alfaro-López, H. M.; Valdés-Madrigal, M. A.; Rojas-Chávez, H.; Cruz-Martínez, H.; Padilla-Islas, M. A.; Tellez-Cruz, M. M.; Solorza-Feria, O. A trimetallic Pt_2NiCo/C electrocatalyst with enhanced activity and durability for oxygen reduction reaction. *Catalysts* **2020**, *10*, 170.

[107] Wang, H. J.; Li, Y. H.; Deng, K.; Li, C. J.; Xue, H. R.; Wang, Z. Q.; Li, X. N.; Xu, Y.; Wang, L. Trimetallic PtPdNi-truncated octahedral nanocages with a well-defined mesoporous surface for enhanced oxygen reduction electrocatalysis. *ACS Appl. Mater. Interfaces* **2019**, *11*, 4252–4257.

[108] Lokanathan, M.; Patil, I. M.; Kakade, B. Trimetallic PtNiCo nanoflowers as efficient electrocatalysts towards oxygen reduction reaction. *Int. J. Hyd. Energy* **2018**, *43*, 8983–8990.

[109] Tinoco-Muñoz, C. V.; Reyes-Rodríguez, J. L.; Bahena-Uribe, D.; Leyva, M. A.; Cabañas-Moreno, J. G.; Solorza-Feria, O. Preparation, characterization and electrochemical evaluation of Ni-Pd and Ni-Pd-Pt nanoparticles for the oxygen reduction reaction. *Int. J. Hyd. Energy* **2016**, *41*, 23272–23280.

[110] Cruz-Martínez, H.; Tellez-Cruz, M. M.; Rojas-Chávez, H.; Ramírez-Herrera, C. A.; Calaminici, P.; Solorza-Feria, O. NiPdPt trimetallic nanoparticles as efficient electrocatalysts towards the oxygen reduction reaction. *Int. J. Hyd. Energy* **2019**, *44*, 12463–12469.

[111] Eid, K.; Wang, H. J.; Malgras, V.; Alothman, Z. A.; Yamauchi, Y.; Wang, L. Trimetallic PtPdRu dendritic nanocages with three-dimensional electrocatalytic surfaces. *J. Phys. Chem. C* **2015**, *119*, 19947–19953.

[112] Deng, Y. Y.; Yin, S. L.; Liu, Y. Y.; Lu, Y. D.; Cao, X. Q.; Wang, L.; Wang, H. J.; Zhao, Y. L.; Gu, H. W. Mesoporous AgPdPt nanotubes as electrocatalysts for the oxygen reduction reaction. *ACS Appl. Nano Mater.* **2019**, *2*, 1876–1882.

[113] Li, K.; Li, X. X.; Huang, H. W.; Luo, L. H.; Li, X.; Yan, X. P.; Ma, C.; Si, R.; Yang, J. L.; Zeng, J. One-nanometer-thick ptnirh trimetallic nanowires with enhanced oxygen reduction electrocatalysis in acid media: Integrating multiple advantages into one catalyst. *J. Am. Chem. Soc.* **2018**, *140*, 16159–16167.

[114] Yan, Y. C.; Du, J. S.; Gilroy, K. D.; Yang, D. R.; Xia, Y. N.; Zhang, H. Intermetallic nanocrystals: Syntheses and catalytic applications. *Adv. Mater.* **2017**, *29*, 1605997.

[115] Kim, H. Y.; Kwon, T.; Ha, Y.; Jun, M.; Baik, H.; Jeong, H. Y.; Kim, H.; Lee, K.; Joo, S. H. Intermetallic PtCu nanoframes as efficient oxygen reduction electrocatalysts. *Nano Lett.* **2020**, *20*, 7413–7421.

[116] Yang, C. L.; Wang, L. N.; Yin, P.; Liu, J. Y.; Chen, M. X.; Yan, Q. Q.; Wang, Z. S.; Xu, S. L.; Chu, S. Q.; Cui, C. H. et al. Sulfur-anchoring synthesis of platinum intermetallic nanoparticle catalysts for fuel cells. *Science* **2021**, *374*, 459–464.

[117] Li, J. R.; Sharma, S.; Liu, X. M.; Pan, Y. T.; Spendelow, J. S.; Chi, M. F.; Jia, Y. K.; Zhang, P.; Cullen, D. A.; Xi, Z. et al. Hard-magnet $L1_0$-CoPt nanoparticles advance fuel cell catalysis. *Joule* **2019**, *3*, 124–135.

[118] Xiao, F.; Wang, Q.; Xu, G. L.; Qin, X. P.; Hwang, I.; Sun, C. J.; Liu, M.; Hua, W.; Wu, H. W.; Zhu, S. Q. et al. Atomically dispersed Pt and Fe sites and Pt-Fe nanoparticles for durable proton exchange membrane fuel cells. *Nat. Catal.* **2022**, *5*, 503–512.

[119] Chong, L.; Wen, J. G.; Kubal, J.; Sen, F. G.; Zou, J. X.; Greeley, J.; Chan, M.; Barkholtz, H.; Ding, W. J.; Liu, D. J. Ultralow-loading platinum-cobalt fuel cell catalysts derived from imidazolate frameworks. *Science* **2018**, *362*, 1276–1281.

[120] Wang, D. L.; Xin, H. L.; Hovden, R.; Wang, H. S.; Yu, Y. C.; Muller, D. A.; DiSalvo, F. J.; Abruña, H. D. Structurally ordered intermetallic platinum-cobalt core–shell nanoparticles with enhanced activity and stability as oxygen reduction electrocatalysts. *Nat. Mater.* **2013**, *12*, 81–87.

[121] Wang, Y.; Zheng, X. B.; Wang, D. S. Design concept for electrocatalysts. *Nano Res.* **2022**, *15*, 1730–1752.

[122] Ji, S. F.; Chen, Y. J.; Wang, X. L.; Zhang, Z. D.; Wang, D. S.; Li, Y. D. Chemical synthesis of single atomic site catalysts. *Chem. Rev.* **2020**, *120*, 11900–11955.

[123] Yang, Z.; Xiang, M.; Zhu, Y. F.; Hui, J.; Jiang, Y.; Dong, S.; Yu, C. B.; Ou, J. F.; Qin, H. F. Single-atom platinum or ruthenium on C_4N as 2D high-performance electrocatalysts for oxygen reduction reaction. *Chem. Eng. J.* **2021**, *426*, 131347.

[124] Wei, X. Q.; Luo, X.; Wu, N. N.; Gu, W. L.; Lin, Y. H.; Zhu, C. Z. Recent advances in synergistically enhanced single-atomic site catalysts for boosted oxygen reduction reaction. *Nano Energy* **2021**, *84*, 105817.

[125] Yang, S.; Tak, Y. J.; Kim, J.; Soon, A.; Lee, H. Support effects in single-atom platinum catalysts for electrochemical oxygen reduction. *ACS Catal.* **2017**, *7*, 1301–1307.

[126] Zhu, X. F.; Tan, X.; Wu, K. H.; Haw, S. C.; Pao, C. W.; Su, B. J.; Jiang, J. J.; Smith, S. C.; Chen, J. M.; Amal, R. et al. Intrinsic ORR activity enhancement of Pt atomic sites by engineering the d-band center via local coordination tuning. *Angew. Chem., Int. Ed.* **2021**, *60*, 21911–21917.